

NUMERICAL SIMULATION OF GERMENCİK GEOTHERMAL FIELD

AHMED HAMENDI

DECEMBER 2009

NUMERICAL SIMULATION OF GERMENCIK GEOTHERMAL FIELD

A THESIS SUBMITTED TO  
GRADUATE SCHOOL OF NATURAL AND APPLIED SCIENCES  
OF  
MIDDLE EAST TECHNICAL UNIVERSITY

BY

AHMED HAMENDI

IN PARTIAL FULFILLMENT OF THE REQUIREMENTS  
FOR  
THE DEGREE OF MASTER OF SCIENCE  
IN  
PETROLEUM AND NATURAL GAS ENGINEERING

DECEMBER 2009

Approval of the thesis:

**NUMERICAL SIMULATION OF GERMENCİK GEOTHERMAL FIELD**

Submitted by **AHMED HAMENDI** in partial fulfilment of the requirements for the degree of **Master of Science in Petroleum and Natural Gas Engineering** by,

Prof. Dr. Canan Özgen \_\_\_\_\_  
Dean, Graduate School of Natural and Applied Sciences

Prof. Dr. Mahmut Parlaktuna \_\_\_\_\_  
Head of Department, Supervisor, Petroleum and Natural Gas Engineering

Prof. Dr. Serhat Akın \_\_\_\_\_  
Co-Supervisor, Petroleum and Natural Gas Engineering, METU

Examining Committee Members:

Prof. Dr. Tanju Mehmetoğlu \_\_\_\_\_  
Petroleum and Natural Gas Engineering, METU

Prof. Dr. Mahmut Parlaktuna \_\_\_\_\_  
Petroleum and Natural Gas Engineering, METU

Prof. Dr. Serhat Akın \_\_\_\_\_  
Petroleum and Natural Gas Engineering, METU

Prof. Dr. Mustafa V. Kök \_\_\_\_\_  
Petroleum and Natural Gas Engineering, METU

Prof. Dr. Nürkan Karahanoğlu \_\_\_\_\_  
Geological Engineering, METU

**I hereby declare that all information in this document has been obtained and presented in accordance with academic rules and ethical conduct. I also declare that, as required by these rules and conduct, I have fully cited and referenced all material and results that are not original to this work.**

Name, Last name: Ahmed HAMENDI

Signature:

# ABSTRACT

## NUMERICAL SIMULATION OF GERMENCİK GEOTHERMAL FIELD

Hamendi, Ahmed

M.Sc., Department of Petroleum and Natural Gas Engineering

Supervisor: Prof. Dr. Mahmut Parlaktuna

Co-Supervisor: Prof. Dr. Serhat Akın

December 2009, 64 pages

The Germencik Omerbeyli geothermal field is considered to be one of the most important geothermal fields in Turkey. A numerical modeling study was carried out to simulate the response of the field to different production/injection scenarios. The reservoir performance evaluation was based on the numerical simulation of the reservoir behavior using the simulation code TOUGH2. The numerical simulation model includes a total area of 85.8 km<sup>2</sup> and extends from the surface at +330 m msl (mean sea level) to a depth of -4581 m msl. Through a trial and error process, the natural state model was satisfactorily matched with the initial temperature and pressure data measured at the wells. The natural state model was further calibrated using the long term flow test (LTFT) data conducted in 2006, including OB-6 and OB-9 as flowing wells and OB-8 as an injection well. The model was then used to predict reservoir performance under different production/injection scenarios over the next 30 years. Forecast runs showed that the pressure declines almost equally in all areas, consistent with the high permeability and connectivity of the reservoir, which had been established from the LTFT.

**Keywords:** Numerical simulation, Germencik geothermal field, TOUGH2

# ÖZ

## GERMENCİK JEOTERMAL SAHASI'NIN SAYISAL SİMÜLASYON

Hamendi, Ahmed

Yüksek Lisans, Petrol ve Doğal Gaz Mühendisliği Bölümü

Tez Yöneticisi: Prof. Dr. Mahmut Parlaktuna

Ortak Tez Yöneticisi: Prof. Dr. Serhat Akın

Aralık 2009, 64 sayfa

Germencik Ömerbeyli jeotermal sahası Türkiye'deki en önemli jeotermal sahalarından biridir. Bu sahanın farklı üretim/enjeksiyon senaryolarındaki tepkisini simüle etmek için sayısal modelleme çalışması yapıldı. Rezervuar performans değerlendirmesi, rezervuar davranışının TOUGH2 simülasyon kodu kullanılarak yapılan sayısal simülasyonuna dayandırılmıştır. Sayısal simülasyon modeli, toplam 85.8 km<sup>2</sup> alanı içermekte ve deniz seviyesinden 330 m yukarıdan deniz seviyesinden 4581 m aşağısına kadar ki derinliği kapsamaktadır. Deneme ve yanılma işlemi boyunca doğal durum modeli, kuyularda ölçülen ilk sıcaklık ve basınç verileriyle tatminkar bir şekilde örtüştü. Doğal durum modeli, OB-6 ve OB-9 kuyuları akış halindeki kuyular, OB-8 kuyusu ise enjeksiyon kuyusu olarak 2006 yılında yapılan Uzun Dönem Akış Testi (LTFT) verilerine kalibre edildi. Bu model daha sonra, önümüzdeki 30 sene içerisindeki farklı üretim/enjeksiyon senaryolarındaki rezervuar performansı tahmininde kullanıldı. Tahmin sonuçları, basıncın, LTFT'den tanımlanan resevuarın yüksek geçirgenliği ve bağlantısallığı ile uyumlu olarak tüm sahalarda eşit miktarda düşmekte olduğunu gösterdi.

**Anahtar kelimeler:** Sayısal simülasyon, Germencik jeotermal sahası, TOUGH2

To The Memory of My Loving Father

## **ACKNOWLEDGEMENTS**

I would like to express my deepest gratitude to both my supervisor Prof. Dr. Mahmut Parlaktuna and co-supervisor Prof. Dr. Serhat Akın for guidance, advice, insight and patience throughout the study.

I would also like to thank my family and friends for their invaluable support and encouragement.

## TABLE OF CONTENTS

ABSTRACT.....	V
ÖZ.....	VI
TABLE OF CONTENTS.....	IX
LIST OF FIGURES.....	XI
LIST OF TABLES.....	XIII
NOMENCLATURE.....	XIV
CHAPTER 1.....	1
INTRODUCTION.....	1
1.1 GEOLOGICAL SETTING.....	1
1.2 GEOCHEMISTRY.....	4
CHAPTER 2 .....	5
LITERATURE REVIEW.....	5
CHAPTER 3 .....	10
STATEMENT OF PROBLEM.....	10
CHAPTER 4.....	11
METHOD OF SOLUTION.....	11
CHAPTER 5 .....	15
RESULTS AND DISCUSSION .....	15
5.1 NUMERICAL RESERVOIR MODEL.....	15
5.1.1 BOUNDARY CONDITIONS.....	21
5.2 INITIAL STATE MODELING.....	22
5.2.1 CALIBRATION.....	23

5.3 2006 LONG TERM FLOW TEST (LTFT).....	28
5.4 FORECASTING.....	33
5.4.1 SCENARIO-1.....	33
5.4.2 SCENARIO-2.....	38
5.4.3 SCENARIO-3.....	42
5.4.4 SCENARIO-4.....	46
5.4.5 SCENARIO-5.....	50
5.5 DISCUSSION.....	54
CHAPTER 6.....	56
CONCLUSIONS.....	56
CHAPTER 7.....	58
RECOMMENDATIONS.....	58
REFERENCES.....	59

## LIST OF FIGURES

<i>Figure 1.1 Location and geological map of Germencik geothermal field.....</i>	<i>2</i>
<i>Figure 1.2 Conceptual model of the Germencik Omerbeyli geothermal field.....</i>	<i>3</i>
<i>Figure 4.1 Method of solution flow chart.....</i>	<i>14</i>
<i>Figure 5.1 Enlarged top view of simulation grid showing well locations.....</i>	<i>17</i>
<i>Figure 5.2 Model grid showing well locations.....</i>	<i>18</i>
<i>Figure 5.3 XZ Cross section of model showing vertical permeability.....</i>	<i>18</i>
<i>Figure 5.4 XZ Cross section of model showing horizontal permeability.....</i>	<i>19</i>
<i>Figure 5.5 YZ cross section of model showing vertical permeability.....</i>	<i>19</i>
<i>Figure 5.6 YZ cross section of model showing horizontal permeability.....</i>	<i>20</i>
<i>Figure 5.7 XY cross section of model showing vertical permeability.....</i>	<i>20</i>
<i>Figure 5.8 XY cross section of model showing horizontal permeability.....</i>	<i>21</i>
<i>Figure 5.9 Model reaching steady state solution.....</i>	<i>22</i>
<i>Figure 5.10 Initial temperature distribution at main production horizon.....</i>	<i>24</i>
<i>Figure 5.11 Three dimensional view of initial pressure distribution.....</i>	<i>24</i>
<i>Figure 5.12 Measured and simulated static temperature profile of well OB-6.....</i>	<i>25</i>
<i>Figure 5.13 Measured and simulated static temperature profile of well OB-8.....</i>	<i>25</i>
<i>Figure 5.14 Measured and simulated static temperature profile of well OB-9.....</i>	<i>26</i>
<i>Figure 5.15 Measured and simulated static pressure profile of well OB-6.....</i>	<i>26</i>
<i>Figure 5.16 Measured and simulated static pressure profile of well OB-8.....</i>	<i>27</i>
<i>Figure 5.17 Measured and simulated static pressure profile of well OB-9.....</i>	<i>27</i>
<i>Figure 5.18 2006 LTFT Production/Injection Data.....</i>	<i>29</i>
<i>Figure 5.19 LTFT OB-3 Simulation Match.....</i>	<i>30</i>
<i>Figure 5.19 LTFT OB-5 Simulation Match.....</i>	<i>31</i>
<i>Figure 5.21 LTFT OB-7 Simulation Match.....</i>	<i>32</i>
<i>Figure 5.22 Simulated reservoir pressure change in scenario-1.....</i>	<i>34</i>
<i>Figure 5.23 Simulated enthalpy change for well OB-3 in scenario-1.....</i>	<i>34</i>
<i>Figure 5.24 Simulated enthalpy change for well OB-5 in scenario-1.....</i>	<i>35</i>

<i>Figure 5.25 Simulated enthalpy change for well OB-9 in scenario-1</i> .....	35
<i>Figure 5.26 Simulated pressure change of production wells in scenario-1</i> .....	36
<i>Figure 5.27 Initial temperature distribution at main production horizon</i> .....	37
<i>Figure 5.28 Final temperature distribution at main production horizon</i> <i>(-1300 m msl) in scenario-1</i> .....	37
<i>Figure 5.29 Simulated reservoir pressure change in scenario-2</i> .....	38
<i>Figure 5.30 Simulated pressure change of production wells in scenario-2</i> .....	39
<i>Figure 5.31 Simulated enthalpy change of production wells in scenario-2</i> .....	40
<i>Figure 5.32 Initial temperature distribution at main production horizon</i> .....	41
<i>Figure 5.33 Final temperature distribution at main production horizon</i> <i>(-1300m msl) in scenario-2</i> .....	41
<i>Figure 5.34 Simulated reservoir pressure change in scenario-3</i> .....	42
<i>Figure 5.35 Simulated pressure change of production wells in scenario-3</i> .....	43
<i>Figure 5.36 Simulated enthalpy change of production wells in scenario-3</i> .....	44
<i>Figure 5.37 Initial temperature distribution at main production horizon</i> .....	45
<i>Figure 5.38 Final temperature distributions at main production horizon</i> <i>(-1300msl) in scenario-3</i> .....	45
<i>Figure 5.39 Simulated reservoir pressure change in scenario-4</i> .....	46
<i>Figure 5.40 Simulated pressure change of production wells in scenario-4</i> .....	47
<i>Figure 5.41 Simulated enthalpy change of production wells in scenario-4</i> .....	48
<i>Figure 5.42 Initial temperature distribution at main production horizon</i> .....	49
<i>Figure 5.43 Final temperature distribution at main production horizon</i> <i>(-1300msl) in scenario-4</i> .....	49
<i>Figure 5.44 Simulated reservoir pressure change in scenario-5</i> .....	50
<i>Figure 5.45 Simulated pressure change of production wells in scenario-5</i> .....	51
<i>Figure 5.46 Simulated enthalpy change of production wells in scenario-5</i> .....	52
<i>Figure 5.47 Initial temperature distribution at main production horizon</i> .....	53
<i>Figure 5.48 Final temperature distribution at main production horizon</i> <i>(-1300msl) in scenario-5</i> .....	53

## LIST OF TABLES

<i>Table 1.1 Wells drilled in Germencik Omerbeyli geothermal field by MTA.....</i>	<i>3</i>
<i>Table 5.1 Simulation model properties.....</i>	<i>23</i>
<i>Table 5.2 Details of production/injection data in scenario 1.....</i>	<i>33</i>
<i>Table 5.3 Details of production/injection data in scenario 2.....</i>	<i>38</i>
<i>Table 5.4 Details of production/injection data in scenario 3.....</i>	<i>42</i>
<i>Table 5.5 Details of production/injection data in scenario 4.....</i>	<i>46</i>
<i>Table 5.6 Details of production/injection data in scenario 5.....</i>	<i>50</i>

# NOMENCLATURE

## Roman

A	Artesian
P	Pressure
T	Temperature
S <sub>g</sub>	Gas phase saturation
P <sub>g</sub>	Gas phase pressure
S	Normalized saturation
S <sub>w</sub>	Composite system water saturation
S <sub>gr</sub>	Composite system residual gas saturation
k <sub>rg</sub>	Gas relative permeability
k <sub>rw</sub>	Water relative permeability
m	exponential term in EFRP equation for water
n	exponential term in EFRP equation for gas
k <sub>m</sub>	Matrix permeability
k <sub>f</sub>	Fracture permeability
P <sub>c,max</sub>	Maximum matrix capillary pressure
V	Velocity

## Greek

μ	Viscosity
μ <sub>w</sub>	Water viscosity
λ	Imbibition index

## Abbreviations

EFRP	Effective fracture relative permeability
GUI	Graphical user interface
LTFT	Long term flow test
MTA	Mineral Research and Exploration Institute of Turkey
TDS	Total dissolved solids
tph	Tons per hour
WHP	Well head pressure

# CHAPTER 1

## INTRODUCTION

The Germencik geothermal field is located in Aydın province in western Turkey, it is considered to be one of the most important geothermal fields of Turkey. The field was discovered by MTA in 1967 and nine wells (OB-1 to OB-9) were drilled between 1982 and 1986 (Table 1.1). There are two main areas of the Germencik geothermal field, the Bozkoy-Camur geothermal field and the Germencik Omerbeyli geothermal field, this study is concerned with the later.

### 1.1 Geological Setting

Simsek (2006), Filiz et al. (2000) and Serpen et al. (2000) conducted a thorough study of the geological setting and geochemical features of the Germencik Omerbeyli geothermal field. The field is located along the northern edge of the East-West trending Buyuk Menderes graben, a tectonically formed large structure extending for 150 km within the Menderes Massif. The Menderes Massif is a large dome like structure, consisting of metamorphic rocks of Paleozoic age and extending 200 km North-South and 150 km East-West in western Anatolia. The geologic setting of the Menderes Massif consists of a paleotectonic era, which includes metamorphism, magmatism and deformation of the main rock formations and a neotectonic era, which is characterized by cross faulting. During the Pliocene and Early Quaternary age, widespread normal faulting caused North-South extensions of the Massif, which resulted in the formation of the graben system.

The basement rocks of the Germencik field are Paleozoic Menderes Massif rocks, which include gneiss, shist, marble and quartzite. As a consequence of the uplift that

caused the graben formation, younger Neogene rocks were deposited over the basement rocks, these include conglomerates, sandstones, claystones and siltstones. The heat source of the geothermal field is considered to be near surface magma intrusion and deep circulation of meteoric waters, which are heated at depth and move along faults and fracture zones to recharge the reservoir.

The Germencik Omerbeyli geothermal field consists of two reservoirs. The first reservoir is comprised of Neogene conglomerates and sandstones. The second reservoir comprises Paleozoic fractured karstic marble, schist, quartzite and gneiss. Each reservoir is overlain by less permeable Neogene aged claystone and mudstone which form the cap rocks. There is however a high degree of hydrological connectivity between the two reservoirs as evidenced by well flow tests.

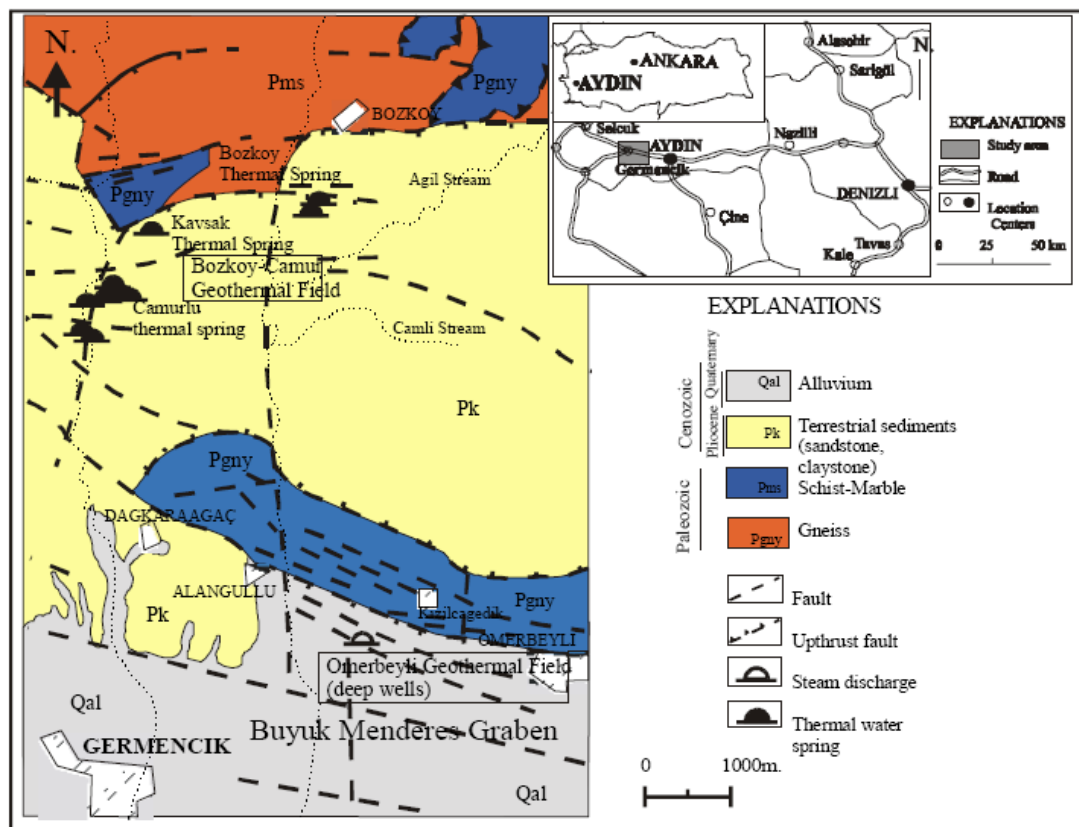


Figure 1.1 Location map, geological map and sections of Germencik geothermal field (Filiz et al, 2000)

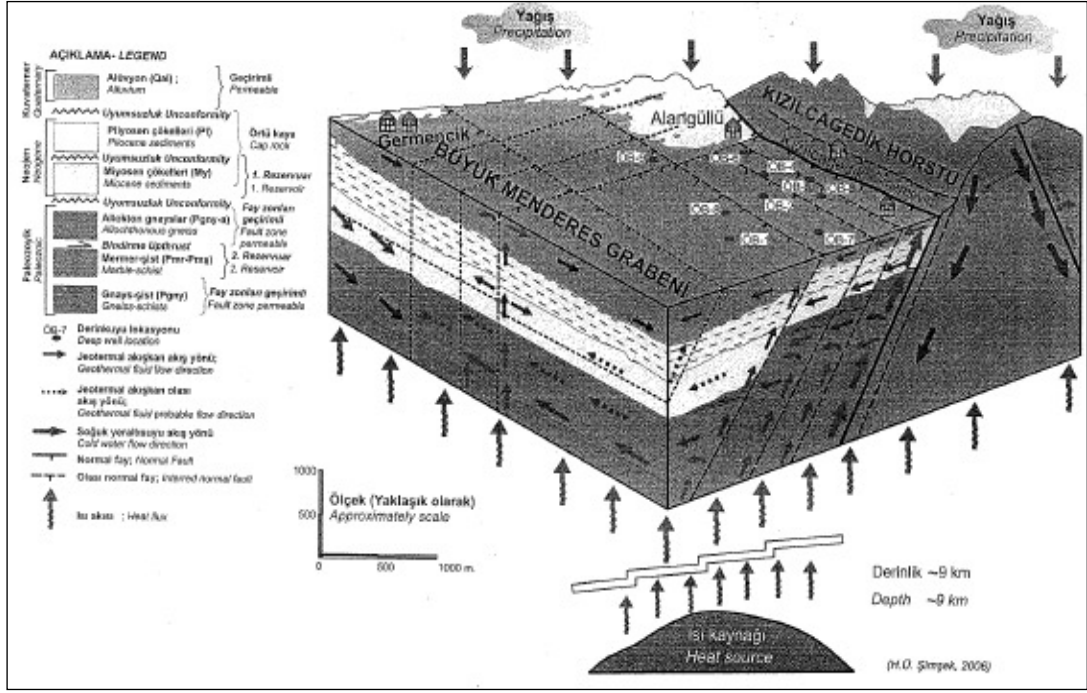


Figure 1.2 Conceptual model of the Germencik Omerbeyli geothermal field (Simsek, 2006)

Table 1.1 Wells drilled in Germencik Omerbeyli geothermal field by MTA (Filiz et al, 2000) (A: Artesian)

Well No.	Date	Depth (m)	Temperature (°C)	Discharge (l/s)	Production Type
OB-1	1982	1002	203	Geyser	Geyser
OB-2	1982	975	231	25	A (4-7 bar)
OB-3	1983	1197	230	65	A (13-15 bar)
OB-4	1984	285	213	180-100	A (15 bar)
OB-5	1984	1270	221	65	A (6 bar)
OB-6	1984	1048	221	140	A (15 bar)
OB-7	1985	2398	203	65	A (2.7 bar)
OB-8	1986	1970	220	120	A (5.4 bar)
OB-9	1986	1460	224	145	A (6.8 bar)

## 1.2 Geochemistry

Several studies have been carried out to investigate the nature and origins of the thermal waters of the Buyuk Menderes graben. The distribution of the thermal systems follow the tectonic patterns of Turkey. The Aegean region in western Turkey is dominated by the rapid westward motion of the Anatolian plate relative to the Eurasia plate, and west to south-westward motion relative to the African plate. The active regimes are concentrated along high strain zones, such as the Buyuk Menderes graben. The large diversity of the ionic composition of geothermal fluids were investigated. Based on the Na/Cl ratio, the geothermal water found in the Germencik field is of non marine Na-HCO<sub>3</sub> type. The authors found that the concentrations of Na, K, Ca, and Mg are largely dependent on the temperature and depth of circulation (Vengosh et al, 2002).

(Simsek, 2003 and Özgür et al, 1998) investigated the chemical and isotopic compositions of samples taken from the Germencik field. The chemical analyses show that the thermal water is of the Na-HCO<sub>3</sub> type which suggests water rock interaction is an important process for most of the chloride hot springs and deep geothermal well fluids in the Germencik reservoirs. The geothermal fluids in the deep reservoirs are of low acidic character. The geothermal water is mainly of meteoric origin. Based on the absence of tritium, the author concludes that the residence time of the water recharging the geothermal system is more than 50 years.

(Ercan and Sahin, 1999) found that the dipolar natural polarization anomalies present in the East West direction along the Germencik Omerbeyli region are not related to surface features. The measurements indicate that besides East West extending fractures, other faults in North South direction also exist. The hottest places were found to be in the junctions and intersections of E-W and N-S trending fault zones.

## **CHAPTER 2**

### **LITERATURE REVIEW**

The literature review will cover a selection of published work dealing with numerical modeling of geothermal reservoirs. In addition, a review of the simulation code used in the study will also be discussed.

The development of numerical simulation models has gone hand in hand with the steady advancement of computing power. The beginning was marked by limited computing power which put many constraints on the numerical models, hence much of the early studies were based on simple geometrical models. As computing power increased, three dimensional models were developed, however, the early work was simplified by including only a small number of grid blocks (O'Sullivan et al, 2001).

As an example of the early work, (Lippmann and Bodvarsson, 1983) carried out a numerical simulation study of the Cerro Prieto geothermal field, the numerical model used was a two-dimensional vertical slice flow model extending from east to west-south-west. In the numerical modeling study of the Heber geothermal field (Lippmann and Bodvarsson, 1985), a two dimensional multilayered axissymmetric (radial symmetry) model was used. These simple models provided limited details of the systems they represent but gave good results for the overall behavior of the system and were used to develop the natural state and exploitation modeling studies. Most of the early three-dimensional models were simplified in some way, usually by omitting low permeability zones entirely (Doughty and Bodvarsson, 1988) or by using a relatively small number of blocks.

All of the major simulation codes have the capability of handling multiphase, multi-component flows. The most widely used simulators today are TOUGH2 (Pruess, 1990b; Pruess et al., 1998), TETRAD (Vinsome and Shook, 1993) and STAR (Pritchett, 1995), SUTRA (Voss, 1984), AQUA (Hu, 1995), GEMMA (Parini et al., 1995), SING (Nakanishi et al., 1995b), SIM.FIGS (Hanano and Seth, 1995) and GEOTHER/HYDROTHERM (Ingebritsen and Sorey, 1985). The advantage of TOUGH2 is that it can handle general unstructured meshes, whereas TETRAD and STAR require a regular rectangular mesh structure (O'Sullivan et al, 2001).

The model calibration process both for natural state modeling and history matching is difficult and time consuming. It is sometimes difficult to decide which part of the model structure should be adjusted to improve the match to a particular field measurement. The use of computerised model calibration (iTOUGH2, Finsterle and Pruess, 1995) has been implemented in improving a few geothermal models (O'Sullivan et al., 1998; White et al., 1998). In this case the computer is used to systematically adjust a few parameters until the differences between model results and field data are at a minimum.

Several models have included a reservoir fluid that is a mixture of water and carbon dioxide (Pruess et al., 1985) or a mixture of water and NaCl (McGuinness et al., 1995) or both (Battistelli et al., 1997). Some models have used tracer test results (Parini et al., 1996), where the tracer test calibrations are particularly useful for calibrating models of highly fractured reservoirs where the rapid return of reinjected water is an important phenomenon.

In some cases production enthalpies from the model can be compared with field data. This process is particularly useful for calibrating the porosity in reservoirs whose wells discharge at two-phase enthalpies (Nakanishi and Iwai, 2000) and for calibrating permeabilities in reservoirs where production temperatures are affected by reinjection returns (Parini et al., 1996).

The complexity of representing naturally fractured rock in a geothermal reservoir has received a great amount of attention. At the present time, four conceptual models have been developed to model naturally fractured reservoirs: 1) dual continuum, 2) discrete fracture network and 3) single equivalent continuum (Sarkar et al, 2000). However, some modelers have simply used a porous medium approach (Gok et al, 2005). while (Yamaguchi et al., 2000) developed an explicit representation of the dominant fractures and faults.

An idealized double porosity model was developed by (Warren and Root, 1963). The double porosity approach idealizes the fracture-flow system as a porous reservoir with homogeneous properties. The rock matrix appears as blocks embedded within this porous aquifer. The blocks have a lower conductivity but a higher storage than the fracture continuum. The authors described two parameters to distinguish the double porosity medium from a homogeneous porous medium, the capacitance of the secondary porosity, which is the porosity of fractures; and a heterogeneity scale index. (Nakanishi and Iwai, 2000) used a double porosity model to develop a simulation model of the Onikobe geothermal field.

Discrete fracture network models describe a class of dual-continuum models in which the porous medium is not represented. Instead, all flow is restricted to the fractures. This idealization reduces computational resource requirements. (Doe et al, 1990) developed a discrete fracture model to flow analysis of dual-porosity systems. The discrete-fracture, dual-porosity approach presented by the authors is an enhancement of discrete fracture network model which associates a volume of storage material with each fracture surface. The flow interactions between the storage volume and the fracture may be either steady-state or transient.

Modeling of heterogeneous naturally fractured reservoirs as a single equivalent system using effective fracture relative permeability (EFRP) was developed by (Babadagli and Ershaghi, 1993). The proposed relative permeabilities developed by the authors are a function of saturation, flow velocity, permeability and capillary pressure in the matrix system.

TOUGH2 (Transport Of Unsaturated Groundwater and Heat 2) is an open architecture multi-dimensional, Integral Finite Difference (IFD) numerical simulator for mass and heat transfer of multiphase, multi-component fluid mixtures in porous and fractured media. The original TOUGH2 code (Pruess, 1990b) provided five Equation of State (EOS) modules (EOS1 to EOS5) to describe the thermophysical properties of fluid mixtures necessary to assemble the governing mass and heat equations. A later modified version of the TOUGH2 code (Pruess et al, 1998) included the previous EOS modules as well as presenting new fluid property EOS modules (see Table 2).

The TOUGH2 code is written in FORTRAN77 and is part of the MULKOM (MULTi-KOMponent) family of codes developed at Lawrence Berkeley Laboratory, in which space discretization is made from the integral form of the basic conservation equations, without converting them into partial differential equations. This integral finite difference (IFD) method (Narasimhan and Witherspoon, 1976) allows regular or irregular discretizations in a multi-dimensional system by avoiding reference to a global system of coordinates. The integral finite difference (IFD) method also allows implementing of double porosity models for fractured media. The discretization results in a set of coupled equations, with the time-dependent primary thermodynamic variables of all grid blocks as unknowns. These equations are then solved simultaneously, using Newton-Raphson iteration. The efficient solution of multiphase flow phenomena can be achieved by automatic time step adjustment (increased or reduced) depending on the convergence rate of the iteration process during a simulation run. The coupled equations arising at each iteration step are then solved by either direct solver method or by the iterative conjugate gradient solver method, with which solutions for large grid systems and three-dimensional problems can be accomplished (Pruess et al, 1999).

The basic Equation of state module is the EOS1 module, it provides a description of pure water in its liquid, vapor, and two-phase states. All the water properties (density, specific enthalpy, viscosity and saturated vapor pressure) are calculated from the steam table equations as given by the International Formulation Committee

(1967). The primary variables are (P, T) for single-phase points and (Pg, Sg) for two-phase points. It is possible to initialize two-phase points as (T, Sg); when the numerical value of the first primary variable is less than 374.15, this will automatically be taken to indicate that this represents temperature rather than pressure. Phase change is recognized through monitoring of the single phase temperature and the corresponding saturation pressure is then compared to the actual fluid pressure. For a liquid point to remain liquid the fluid pressure must be less than the saturation pressure, if this is not satisfied then a transition to two phase conditions takes place (Pruess et al, 1999).

## **CHAPTER 3**

### **STATEMENT OF PROBLEM**

Coupled heat and mass transfer in the highly heterogeneous environment of a geothermal reservoir is a very complex physical process. Often phase changes are involved and often the flow is complicated by the presence of additional chemical species such as gases or dissolved salts. Fundamental research studies have resulted in a steady advance of the range of physical phenomena that it is possible to include in a geothermal reservoir model, and in improvements in the numerical techniques used in the reservoir simulators. These advances have been quite quickly adopted by geothermal modelers. Thus, some models have used reservoir fluid containing various chemicals and others have included extra features such as a numerical representation of double porosity behavior.

The aim of this work is to determine an optimum development scenario for the Germencik Omerbeyli geothermal field, by developing a numerical model using TOUGH2 simulator. For the natural state modeling phase of the study, the model will be calibrated with the temperature and pressure data initially measured at the wells. The numerical model will further be calibrated with the 2006 long term flow test (LTFT) to determine whether the measured vs. modeled data have a satisfactory fit. The last part of this study will involve running several different development scenarios in order to reach least enthalpy decline and most effective pressure support for the reservoir.

## **CHAPTER 4**

### **METHOD OF SOLUTION**

The numerical simulation model was developed in stages; this approach allows various aspects of the model components to be modified as necessary until the match between measured and calculated data is optimized. The Graphical User Interface (GUI) Petrasim was used throughout the study, it is an interactive pre- and post-processor with the ability to create reservoir models and display simulation results through time for the TOUGH2 simulation program.

The stages of the numerical simulation study are:

1. Model grid development
2. Input of model components
3. Natural state modeling
4. Matching of initial state conditions
5. Matching of 2006 long term flow test data
6. Forecast scenarios

#### **1) Model grid development**

The first step in the simulation study was to develop a model grid of the field based on the geology and conceptual model. The grid system is oriented parallel to the Omerbeyli fault, where elevated temperatures are assumed to terminate. Three faults extend from the bottom of the reservoir down into the source up flow area. They provide the conduit for flow of hot geothermal fluid into the reservoir. The model consists of grid blocks of various densities with the finest grid distribution in the area of the well field, such that each well was assigned a unique grid cell block.

## **2) Input of model components**

In this stage, the model components, such as permeability distribution, fluid and heat source location, boundary conditions and thermal properties of the geothermal fluid are entered in to the model. The model components were chosen to be consistent with the conceptual model. However, the geothermal fluid is assumed to be pure water, with no dissolved gas and no dissolved solids.

## **3) Natural state modeling**

It is known that geothermal reservoirs evolve over geologic time. The rate at which thermodynamic conditions change in the natural state are minimal compared to changes induced by reservoir exploitation. Thus, the natural state of a geothermal reservoir is considered to be in quasi-steady state conditions (Bodvarsson et al, 1986). Therefore, the next stage was to run the model with EOS1 executable for 20,000 years to reach a quasi-steady state condition.

## **4) Matching of initial state conditions**

The matching process included modifying the model parameters until the modeled and measured data match sufficiently before moving to the next phase of the calibration process. The initial measured temperature and pressure profile of three wells (OB-6, OB-8 and OB-9) were available for this process.

## **5) Matching of 2006 long term flow test (LTFT)**

The next phase of the calibration was to match the results of the long term flow test (LTFT) conducted in May of 2006. The matching of the modeled and measured LTFT production and injection response required several modifications after the initial state match.

## 6) Forecasting

Once the model has provided satisfactory matching results, the next step is forecasting. Five development scenarios were selected for numerical simulation. The simulation time for all scenarios is 30 years except scenario-1.

- Scenario-1: consists of a 10 year depletion case scenario, with a total production of 2420 tph from wells drilled in the center of the field.
- Scenario-2: the wells OB-14, OB-17 and Ob-19 drilled in the eastern edge of the reservoir are introduced to the model to be used as injectors. The producing wells are the same as those used in scenario-1.
- Scenario-3: At this stage, the Alangulu wells (AG 22-26) are entered in to the model, to be used together with Ob-9 as injectors. The total production assigned to the producing wells (OB-5, OB-6, OB-10, OB-11, OB-14 and OB-17) is 2520 tph, while total injection is held at 2015 tph with 441 kJ/kg enthalpy, corresponding to 105°C. The mass ratio of injection to production is held at 0.8
- Scenario-4: the same production and injection data from scenario-3 are continued with the addition of OB-8 as an injector.
- Scenario-5: the same production and injection data from scenario-3 are used. However, injection is limited to the Alangulu wells, while OB-8 and OB-9 are not used for injection.

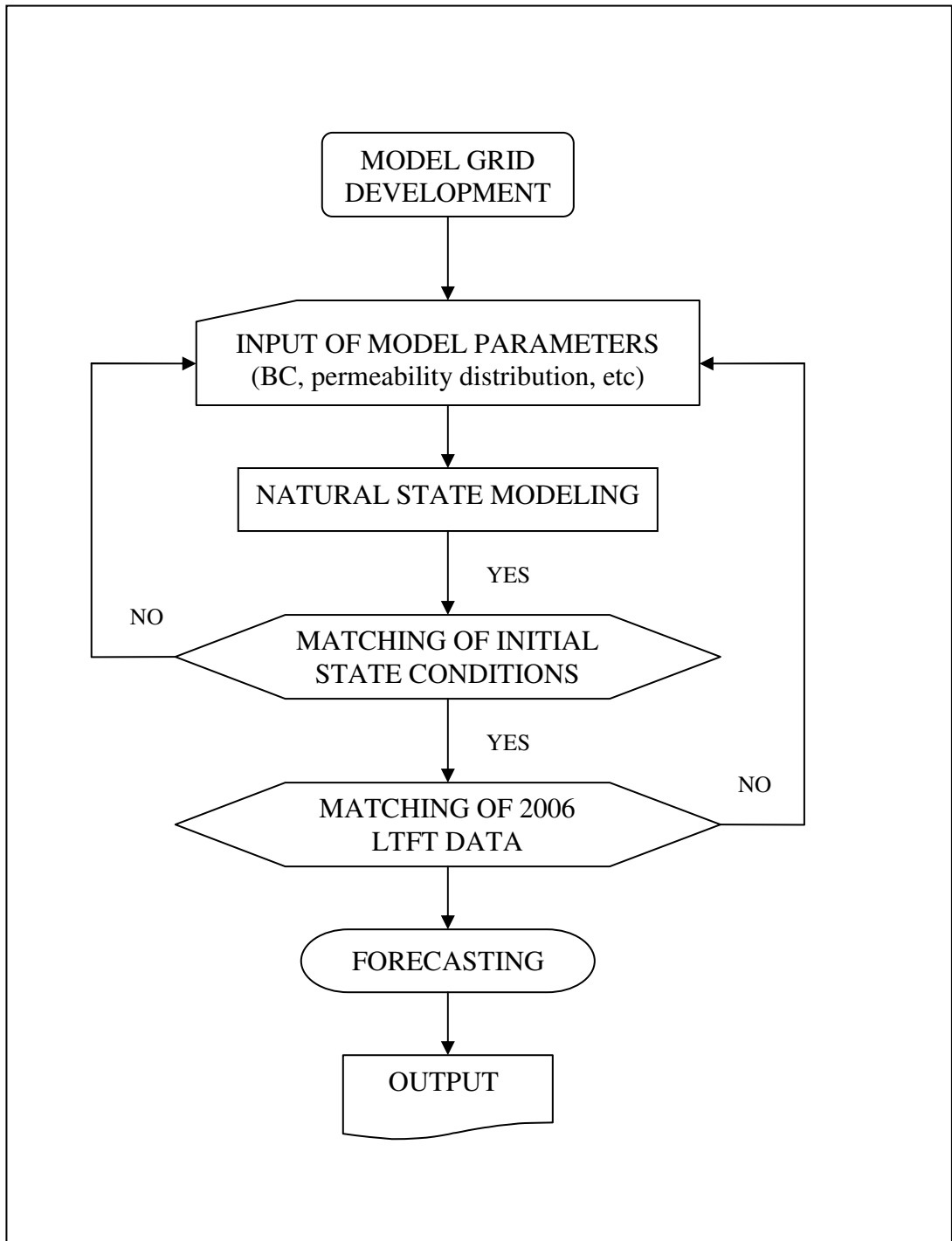


Figure 4.1 Method of solution flow chart

## **CHAPTER 5**

### **RESULTS AND DISCUSSION**

#### **5.1 Numerical reservoir model**

A three dimensional numerical model of the Germencik Omerbeyli geothermal field was developed in TOUGH2 (Pruess et al, 1999) format. The numerical model was based on the conceptual model of the field (Simsek, 2006), as such that the grid system is oriented parallel to the Omerbeyli fault, which forms a hydrogeologic boundary of the system. The grid system consists of a total of 35,475 grid blocks. There are 15 layers and each layer contains 2365 grid blocks, such that the finest grid is in the area of the well field, and where each well was assigned a unique grid cell. The layers of the model are curved to match the stratigraphy of the different geologic units. The simulation grid includes a total area of 85.8 km<sup>2</sup>, and measures 7,8 km in the x direction and 11 km in the y direction.

The permeability distribution for the model was assigned using the simplest assumptions that were consistent with the conceptual model. In order to match the initial conditions in the reservoir, the permeability was varied iteratively to reach the best possible match between stimulated and measured static surveys. The horizontal permeability is 5 to 12 times the vertical permeability. The faults are distinguishable on permeability cross sections as high horizontal and vertical permeability zones. The system was assigned an augmented porosity of 10%.

The reservoir system was treated to behave as a single equivalent system (Babadagli and Ershaghi, 1993), which allows a naturally fractured reservoir to be represented as a single system by introducing an effective fracture relative permeability (EFRP).

The effective fracture relative permeability (EFRP) represents the relative permeability of the composite system (matrix and fracture). The effective fracture relative permeabilities curves are based on the recovery curves obtained from the performance of composite systems under the capillary interaction between the matrix and fracture. The following relationships were found to be applicable (Babadagli and Ershaghi, 1993).

$$S = \frac{S_w - S_{wi}}{1 - S_{wi} - S_{gr}}$$

$$k_{rg} = (1 - S^n)$$

$$k_{rw} = S^m$$

The exponential (n) for gas relative permeabilities and exponential (m) for liquid relative permeabilities are calculated as shown below,

$$\log(n) = (-0.11139(\log(1/\lambda^2))^2 - (0.3421)(\log(1/\lambda)) - 0.1863$$

$$\log(m) = (0.0604)(\log(1/\lambda))^2 - (0.2999)(\log(1/\lambda)) + 0.2554$$

Where  $\lambda$ , a dimensionless group, is called the imbibition index,

$$\lambda = \frac{P_{c, \max} k_m}{V \mu_w \sqrt{k_f}}$$

The imbibition index is a measure of the capillary imbibition performance. As the index  $\lambda$  increases, caused by lower rates or higher ( $P_{c, \max} k_m$ ) product, the capillary imbibition increases. At very high rates or low ( $P_{c, \max} k_m$ ), the imbibition index and the imbibition performance decrease.

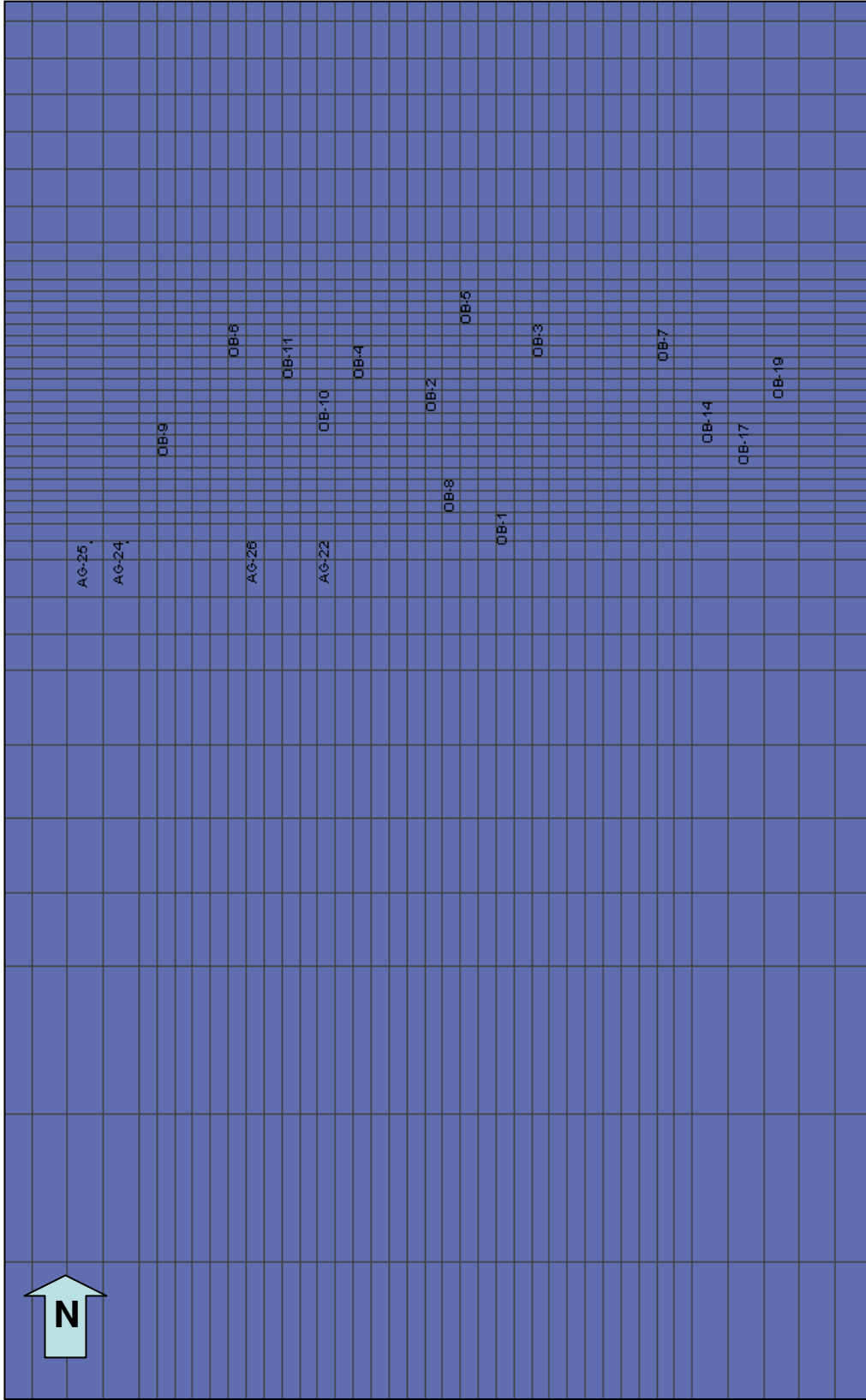


Figure 5.1 Enlarged top view of simulation grid showing well locations

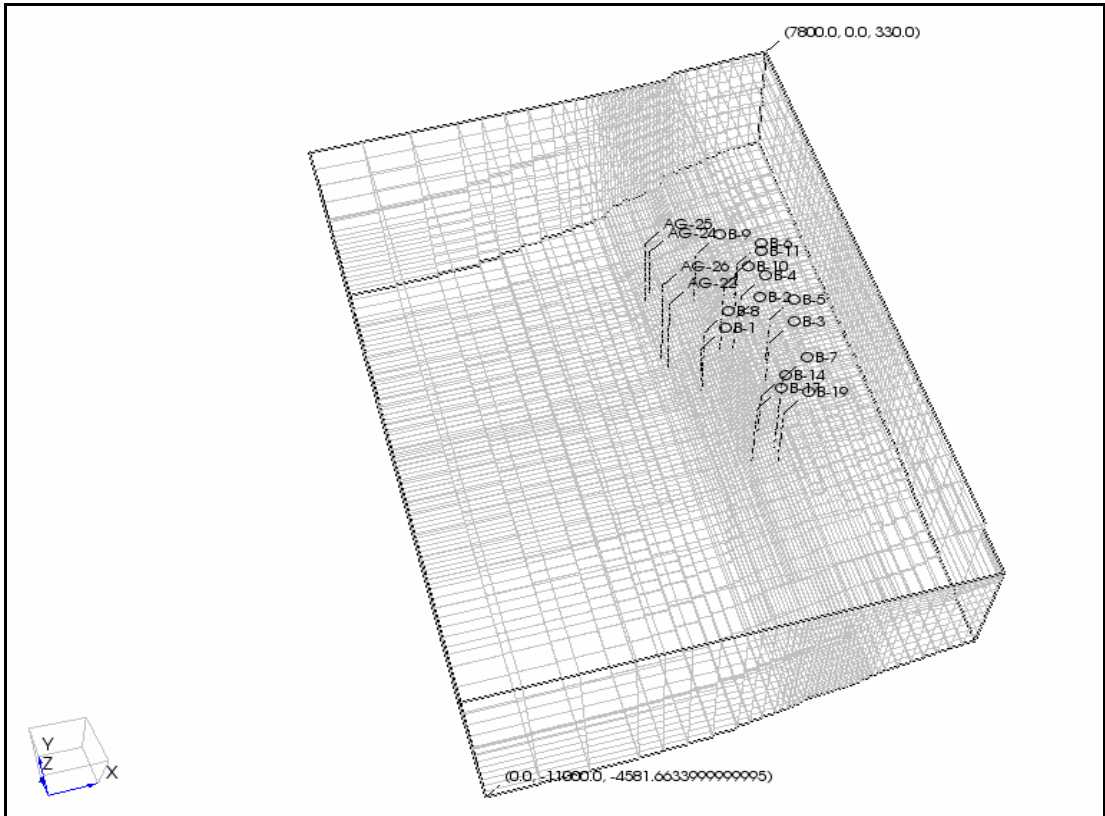


Figure 5.2 Model grid showing well locations

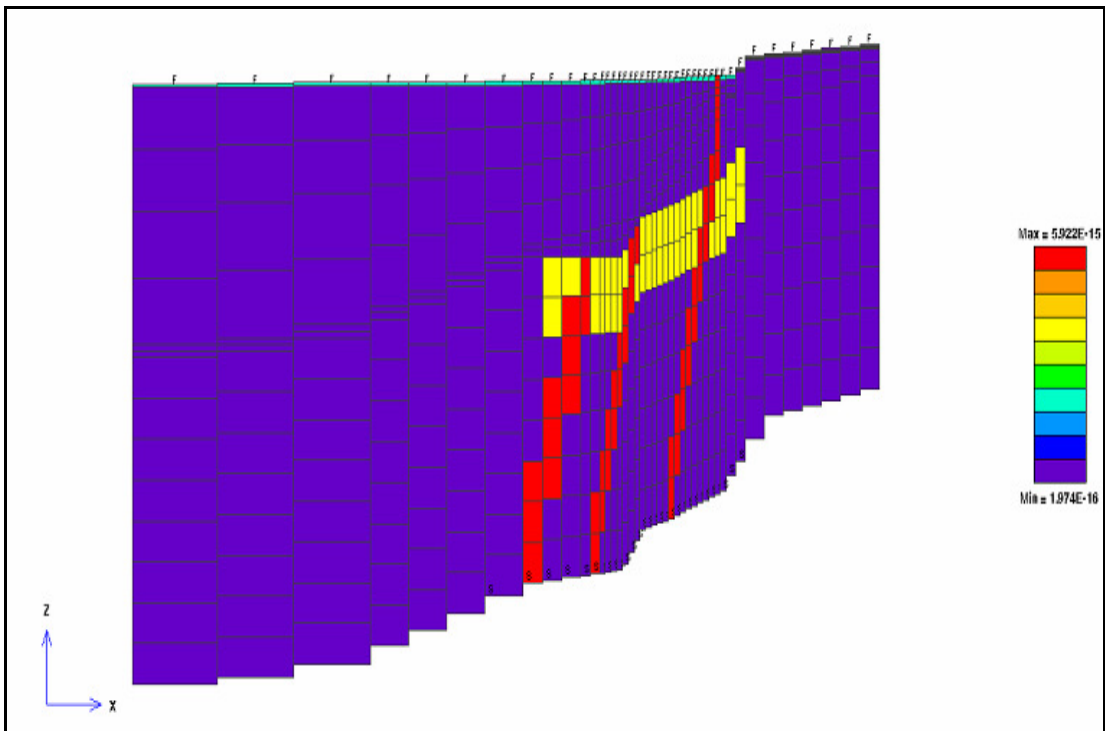


Figure 5.3 XZ Cross section of model showing vertical permeability (millidarcies)

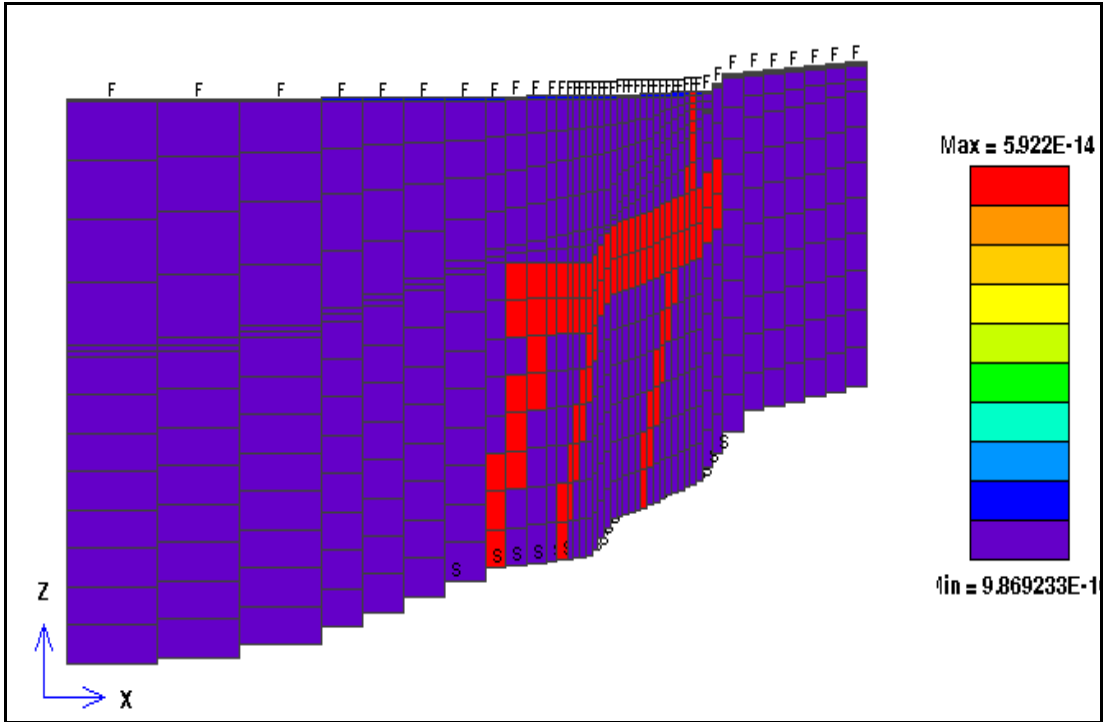


Figure 5.4 XZ Cross section of model showing horizontal permeability (millidarcies)

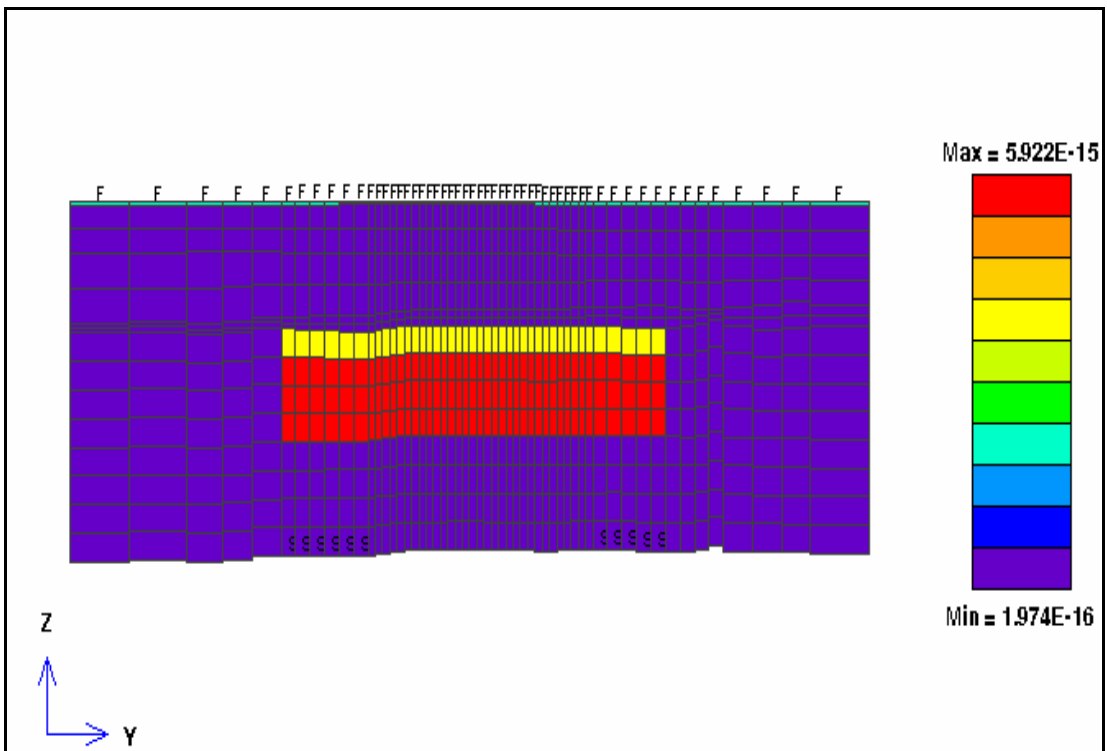


Figure 5.5 YZ cross section of model showing vertical permeability (millidarcies)

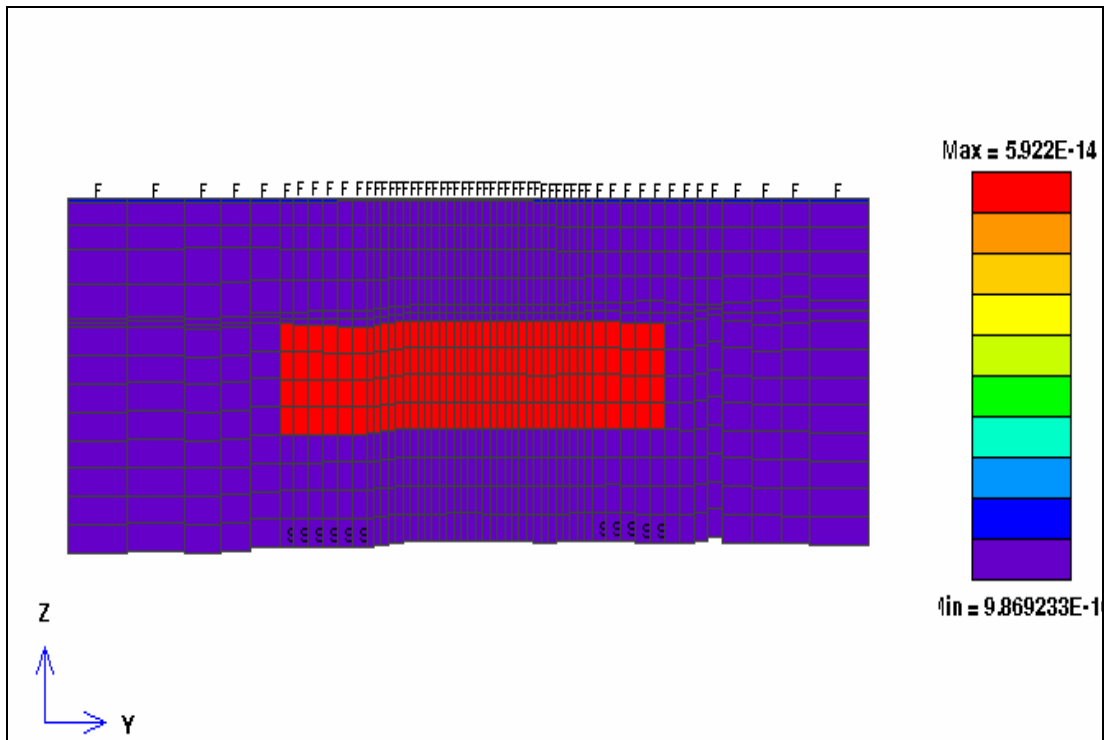


Figure 5.6 YZ cross section of model showing horizontal permeability (millidarcies)

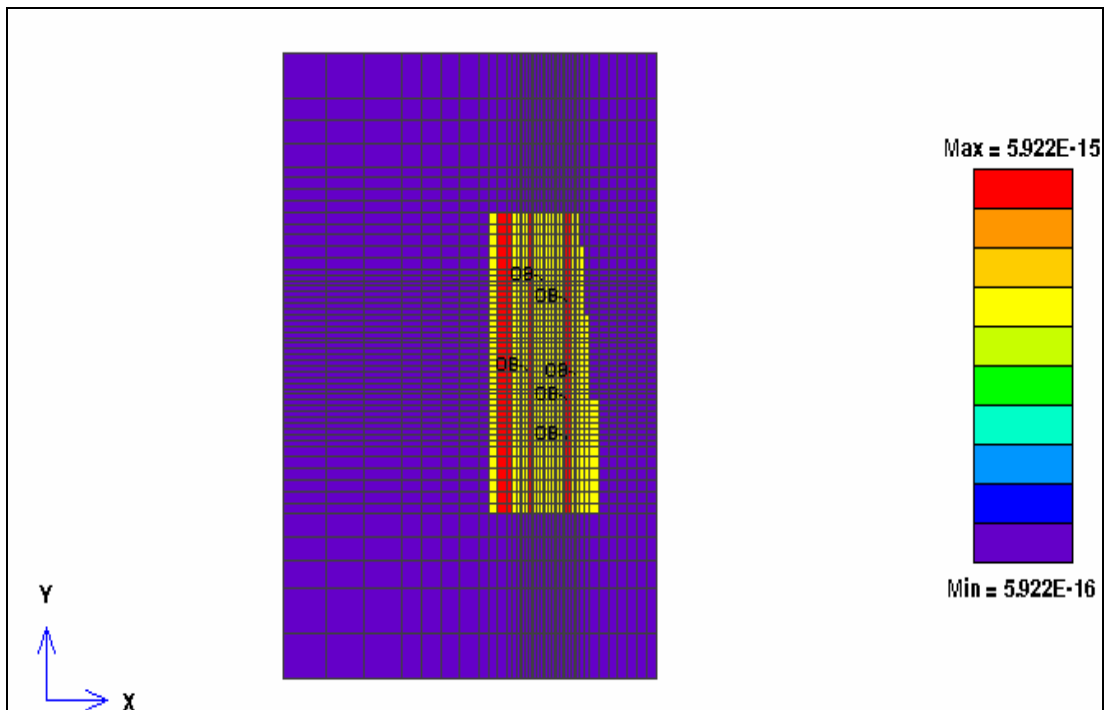


Figure 5.7 XY cross section of model showing vertical permeability (millidarcies)

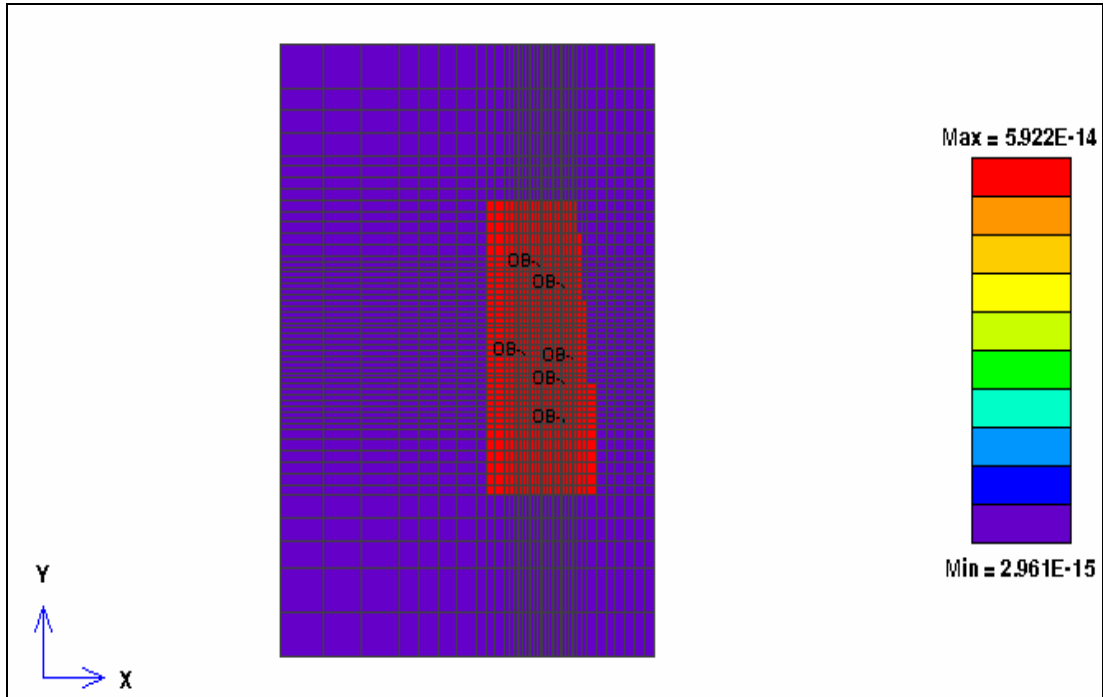


Figure 5.8 XY cross section of model showing horizontal permeability (millidarcies)

### 5.1.1 Boundary conditions

Assumptions regarding initial state boundary conditions include the physical nature of the edge of the field such as whether mass, pressure or heat is transferred across a boundary. For the initial state model the following boundary conditions were used:

- The source fluid inflow is 300 tph with an enthalpy of 1042 kJ/kg (241°C) at the base of the model. This source inflow is not increased during production.
- Outside the source inflow area, there is a conductive inflow of heat that is equivalent to a temperature gradient of 50 °C/km. This was accomplished by assigning a constant temperature boundary condition.
- The remaining sides of the model are all no flow boundaries with respect to mass and heat flow.

- The top of the model was assigned a constant temperature and pressure value with heat loss to an ambient temperature of 30 °C and atmospheric pressure (1 bar). The fumarole near well OB-4 was neglected due to the negligible effect on the overall system.

## 5.2 Natural state modeling

To reach the initial state condition of the field before exploitation, the model was allowed to run for 20,000 years to reach a quasi steady state condition (figure 5.5). The model was run with EOS1 executable, assuming pure water as the geothermal fluid with no CO<sub>2</sub> gas and no dissolved solids. After numerous iterations, varying the permeability distribution and the boundary conditions, a match was obtained between the measured and calculated data. The model properties used in the simulation are shown in table 5.1.

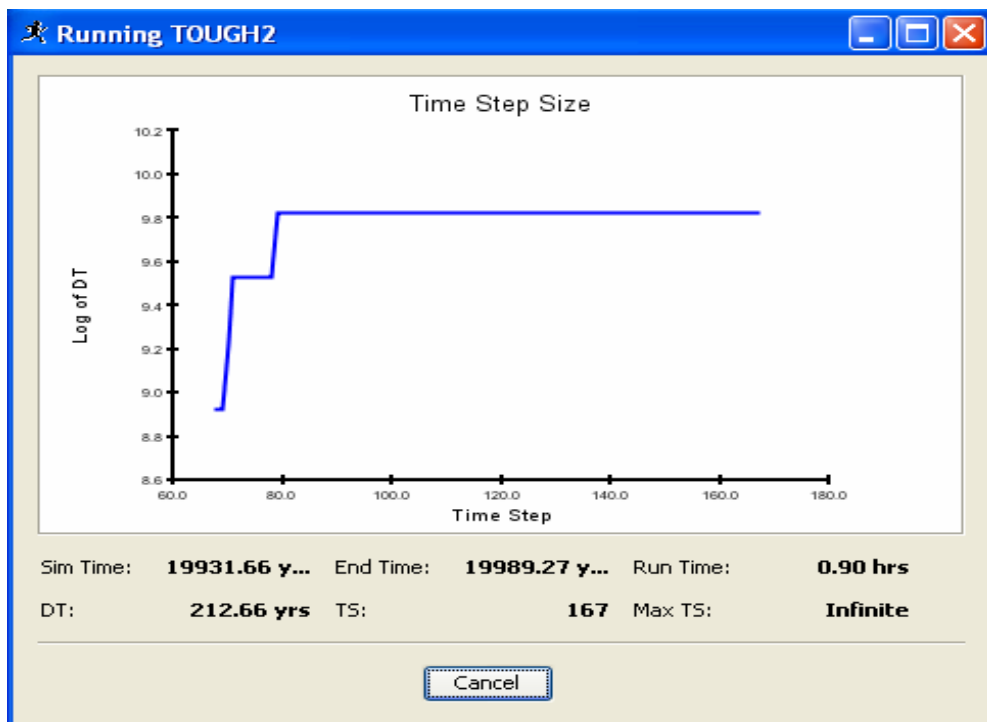


Figure 5.9 model reaching steady state solution

Table 5.1 Simulation model properties

<b>Proeprty</b>	<b>Value</b>
Rock density	2600 kg/m <sup>3</sup>
Wet heat conductivity	2 W/m-C
Specific heat	1000 J/kg-C
Effective fracture realtive permeability	m = 1.58, n = 0.52
Capillary pressure	4 psi

### 5.2.1 Calibration

The first step of the calibration process is the matching of the measured static temperature data of the wells. The subsurface temperature data available is quite limited. The matching process includes the only available data, which are the temperature profiles of OB-6, OB-8 and OB-9 wells. In this step of the modeling process, the initial state numerical model was modified iteratively by trial and error method until a match between the modeled and measured static temperature profiles was obtained. The temperature reversals in the deepest entries of OB-8 and OB-9 suggest that elevated temperatures do not extend at depth in the west. In general, the modeled and measured temperature surveys match reasonably well.

Matching of the static pressure profiles of the same wells, OB-6, OB-8 and OB-9 was also carried out. The figures show that a good matched was obtained. However, there is not enough data to make any interpretations about the changes in slope that are seen at approximately 800 meters. The changes in slope at shallow depths of a few hundred meters, however, might be attributed to the effect of free gas in a two-phase zone, which reduces the pressure gradient.

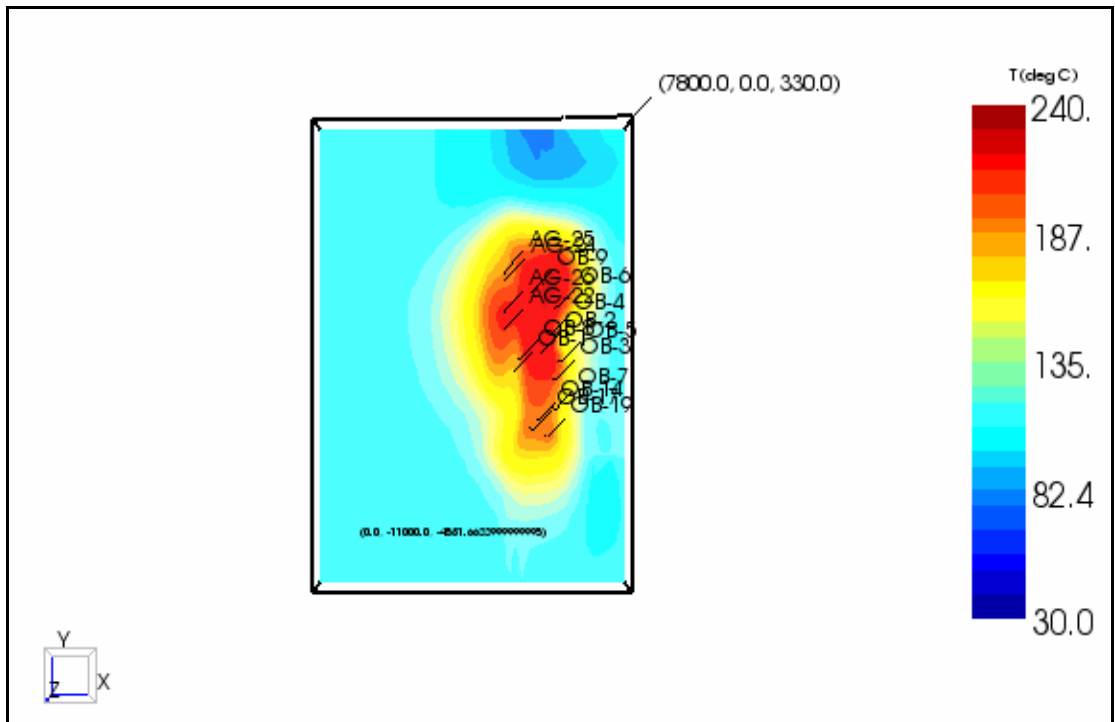


Figure 5.10 Initial state simulated temperature distribution at main production horizon (-1300m msl)

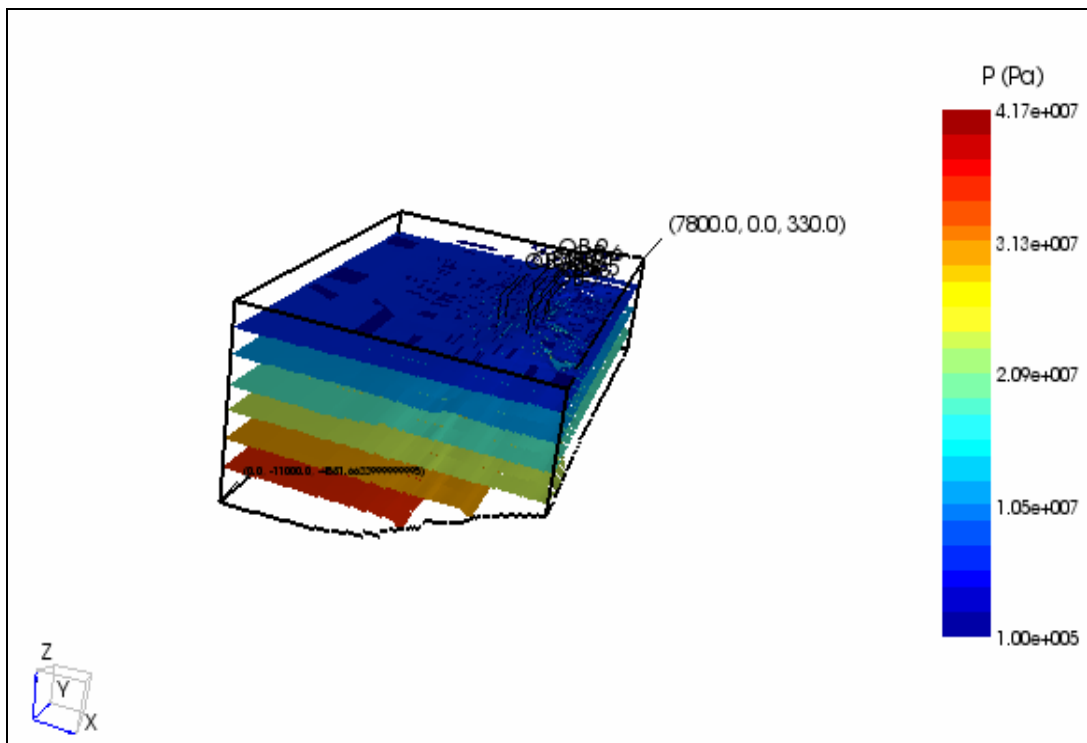


Figure 5.11 Three dimensional view of initial pressure distribution

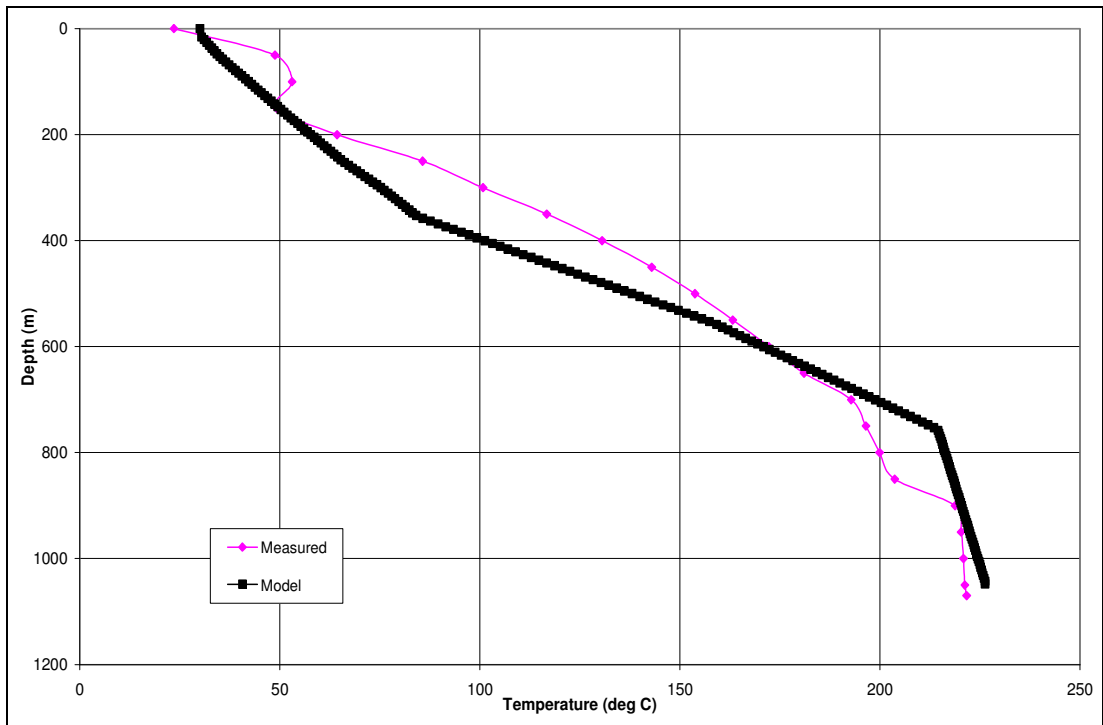


Figure 5.12 Measured and simulated static temperature profile of well OB-6

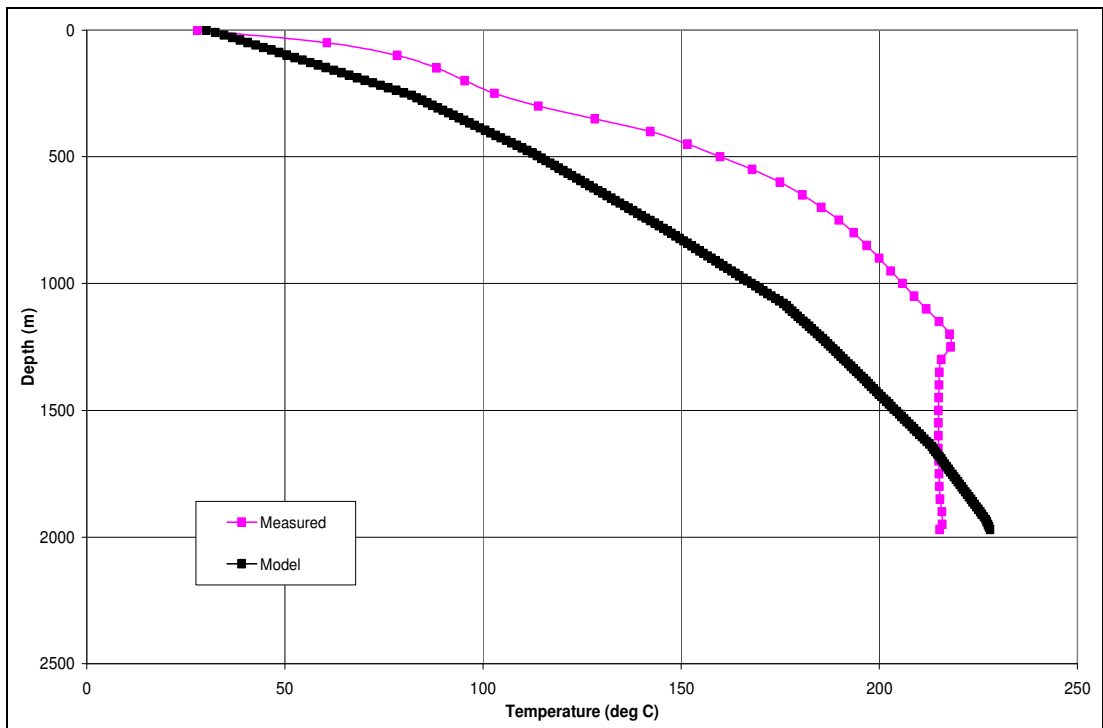


Figure 5.13 Measured and simulated static temperature profile of well OB-8

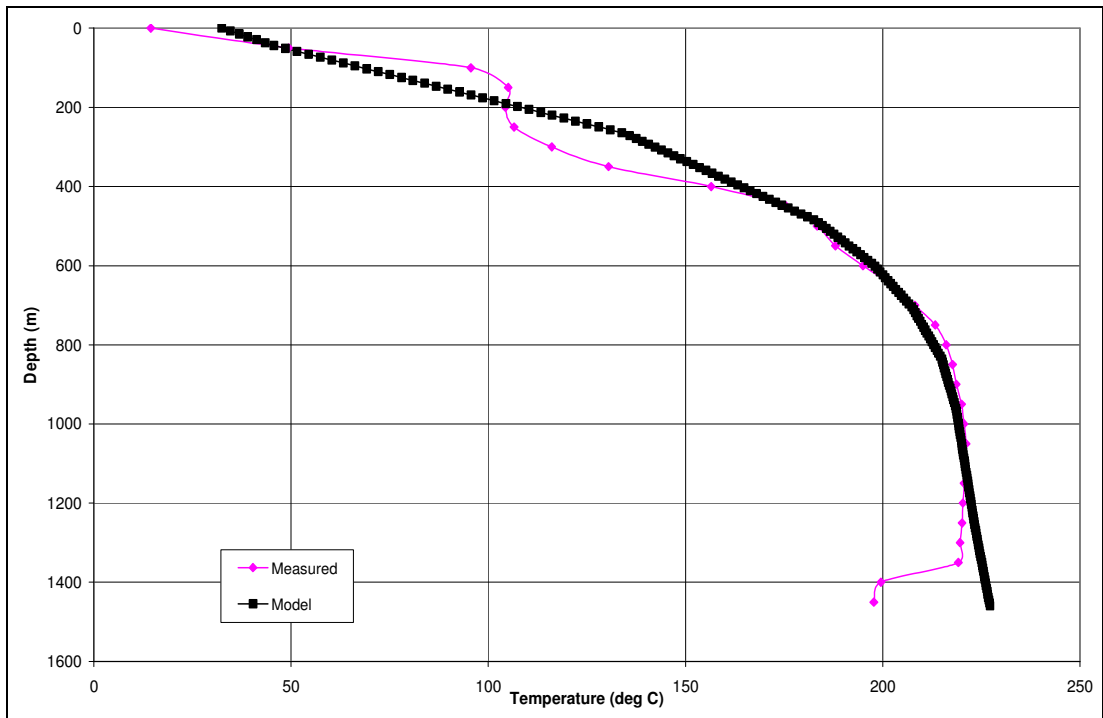


Figure 5.14 Measured and simulated static temperature profile of well OB-9

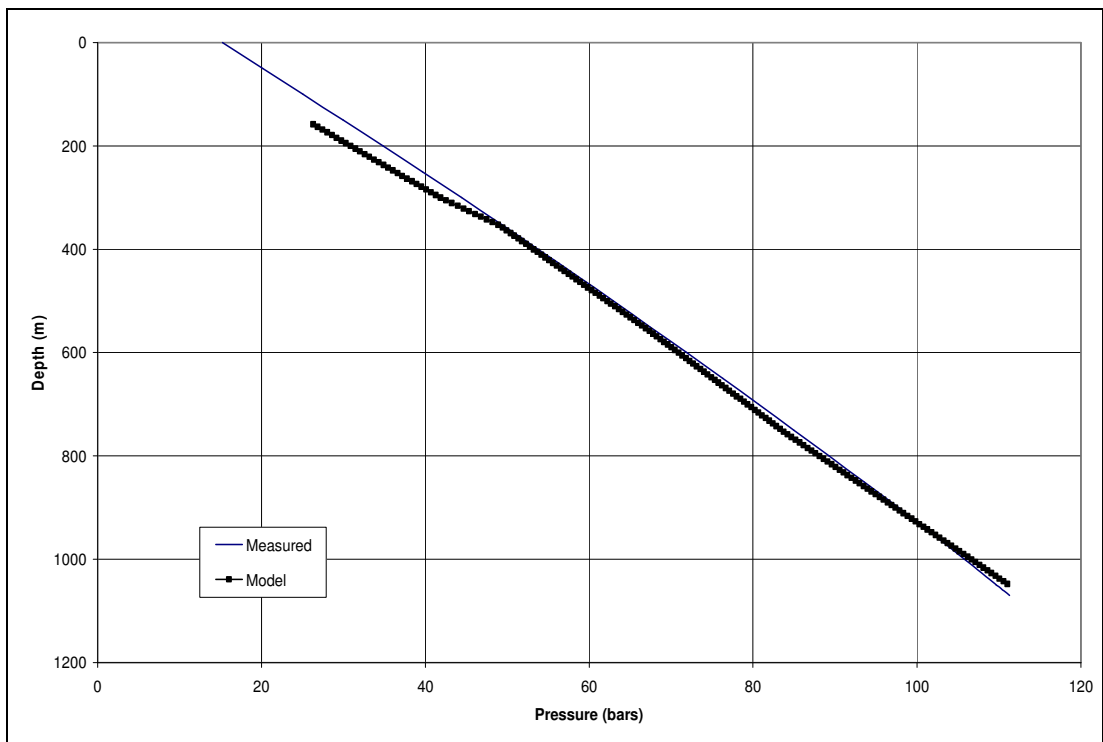


Figure 5.15 Measured and simulated static pressure profile of well OB-6

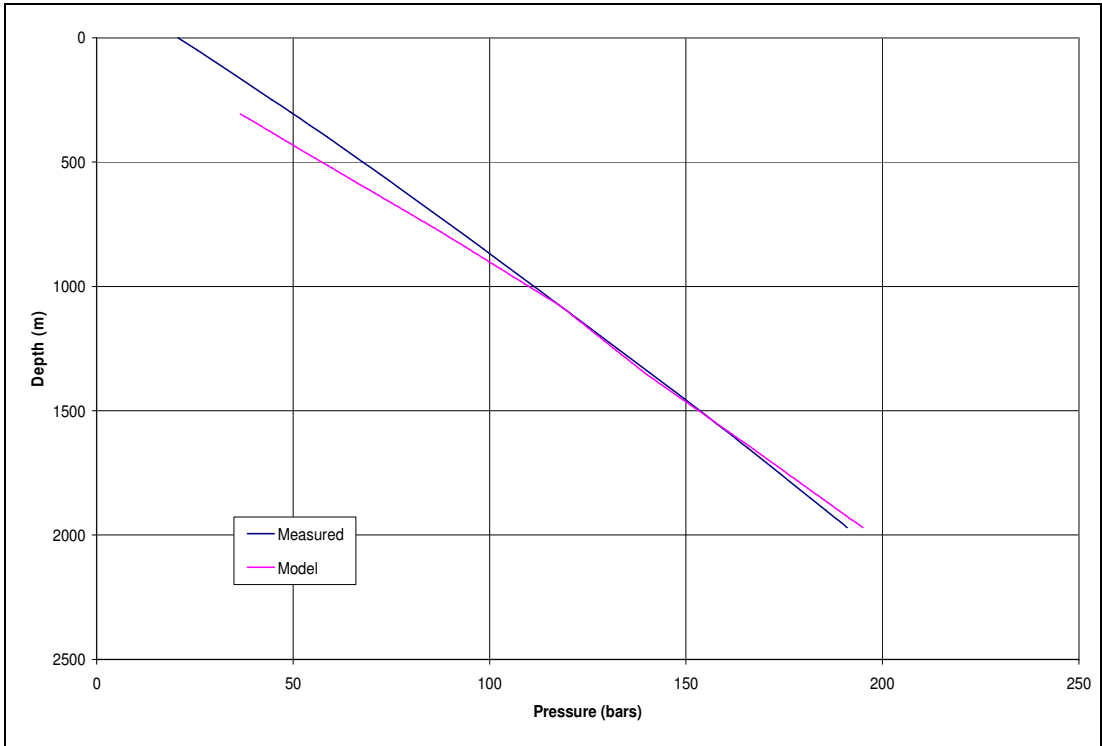


Figure 5.16 Measured and simulated static pressure profile of well OB-8

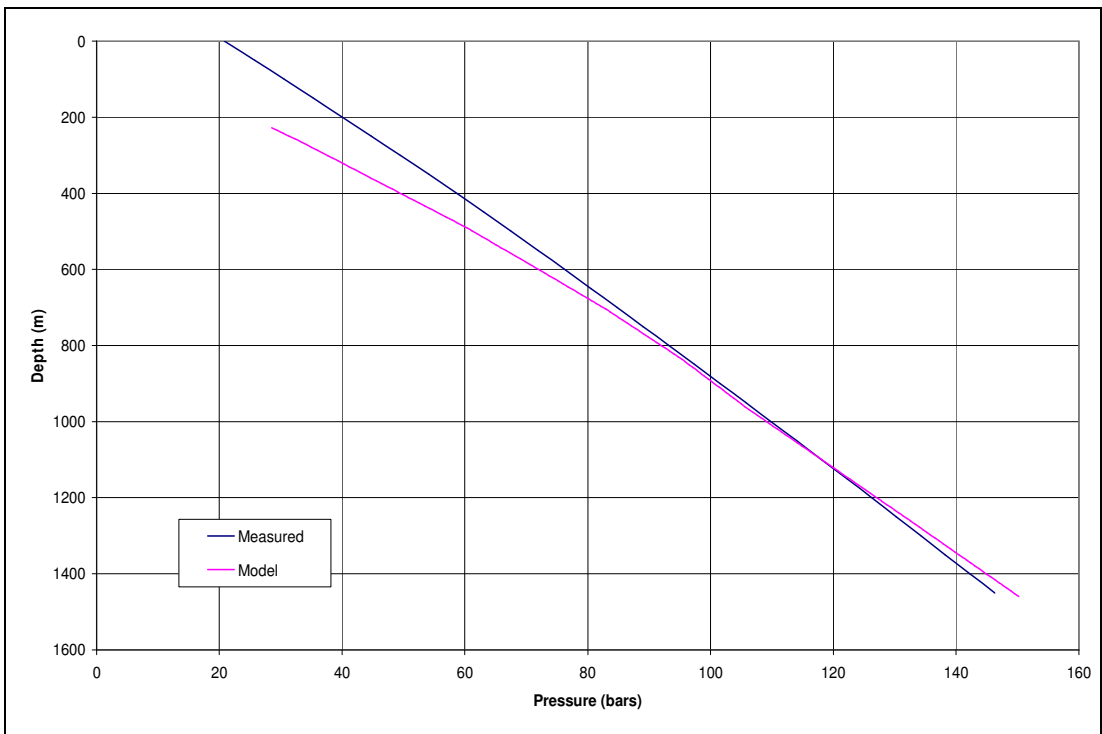


Figure 5.17 Measured and simulated static pressure profile of well OB-9

### **5.3 2006 Long Term Flow Test (LTFT)**

A long term flow test (LTFT) for the Germencik geothermal field was performed during April and May 2006. The test included the wells OB-6 and OB-9 for production, OB-8 as an injection well, and OB-3, OB-5 and OB-7 as monitoring wells. The data obtained from the LTFT was used to perform history matching between measured and modeled pressure response to further calibrate the simulation model.

For the duration of the LTFT, the wells OB-6 and OB-9 were produced for 40 days starting from April 4th and shut-in for 45 days on May 14th, while OB-8 was introduced as an injection well on the 12th day of the test. For the duration of the test, the bottomhole pressure was monitored at wells OB-3, OB-5 and OB-7.

During stabilized flow, OB-6 produced between 290-310 tph with well head pressure (WHP) between 25-27 kg/cm<sup>2</sup> and a flowing enthalpy of 929 kJ/kg. The well OB-9 produced between 260-300 tph with WHP between 22-25 kg/cm<sup>2</sup> and a flowing enthalpy of 892 kJ/kg. Injection into OB-8 stabilized at approximately 240 tph with WHP at 26 kg/cm<sup>2</sup>.

There was no decline in the deliverability of the wells over the testing period. The monitoring wells OB-3, OB-5 and OB-7 showed rapid pressure response to production and injection, which indicates that the reservoir permeability is continuous over the well field area. The results of the test also suggest that injection will be critical to support reservoir pressure decline, but must be carefully managed to prevent thermal breakthrough.

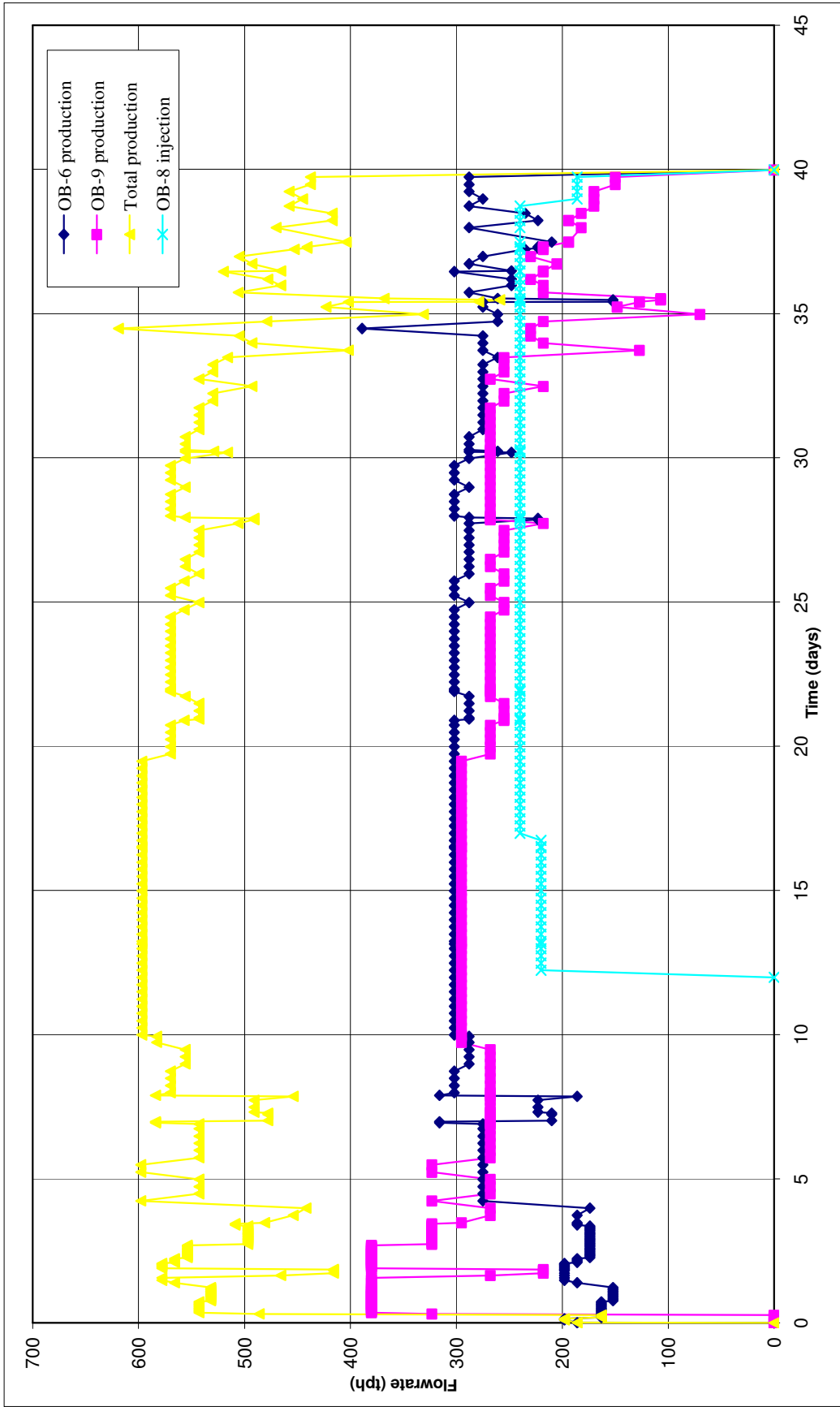


Figure 5.18 2006 LTFT production/injection data

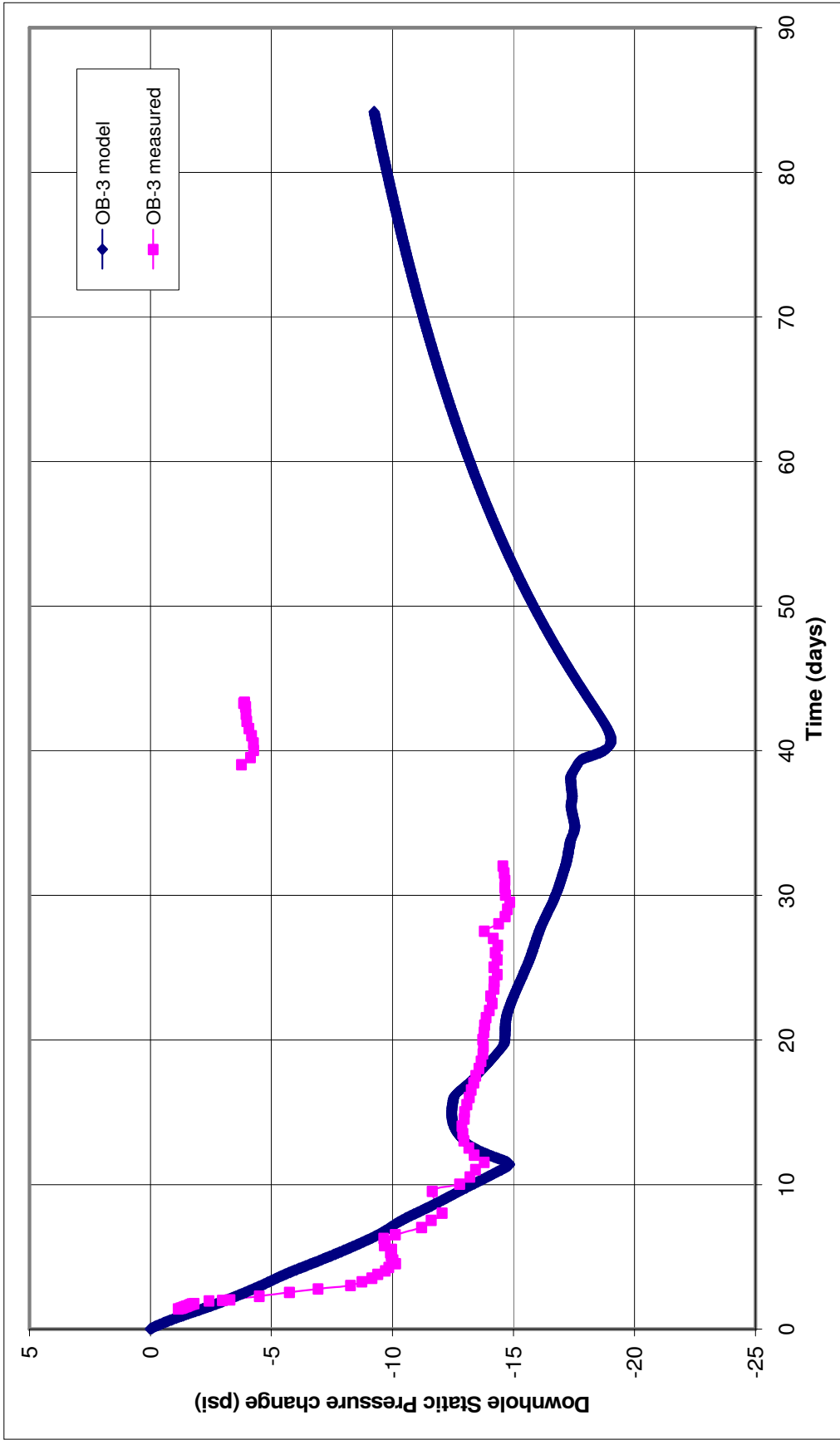


Figure 5.19 LTFT OB-3 Simulation Match

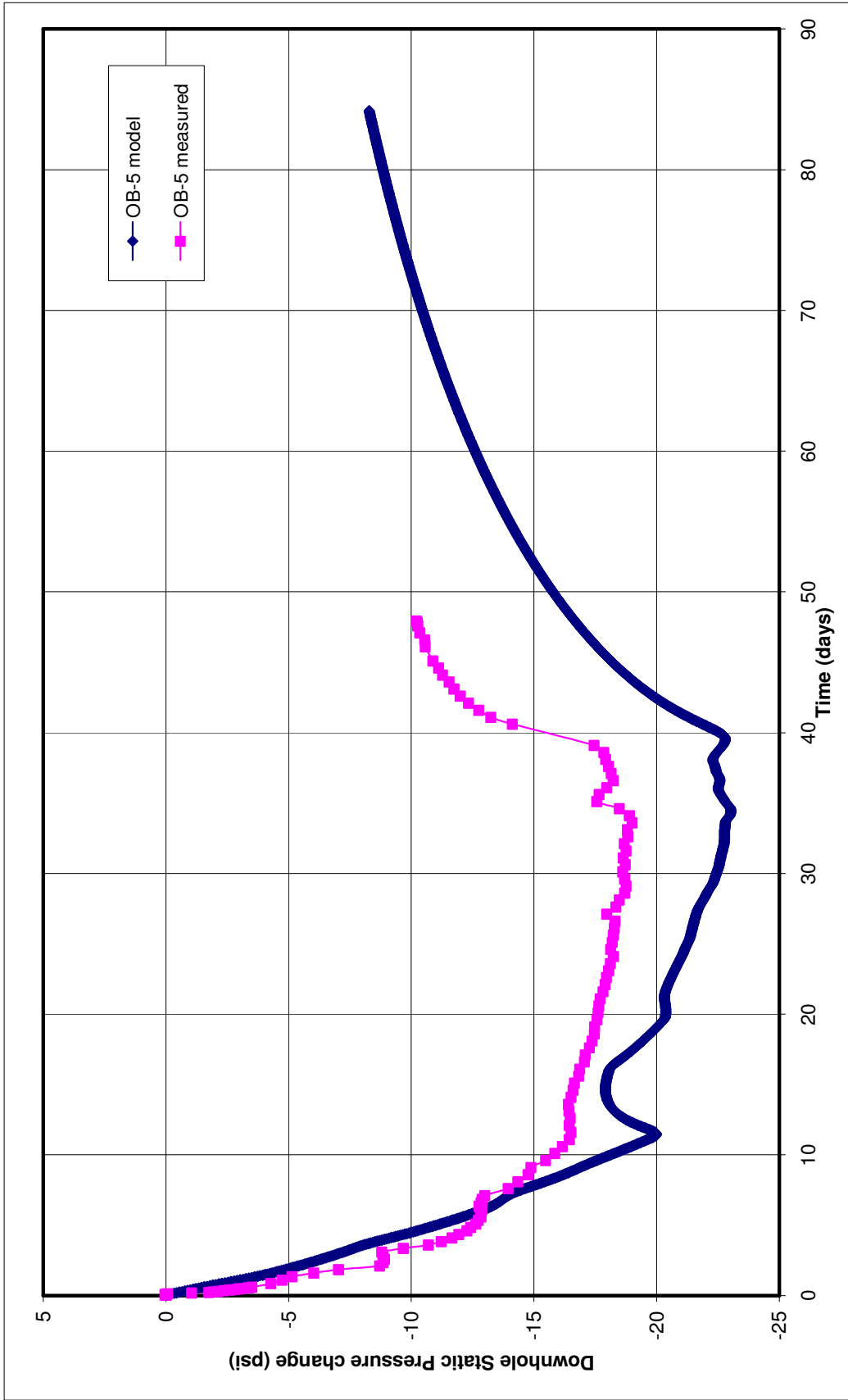


Figure 5.20 LTFT OB-5 Simulation Match

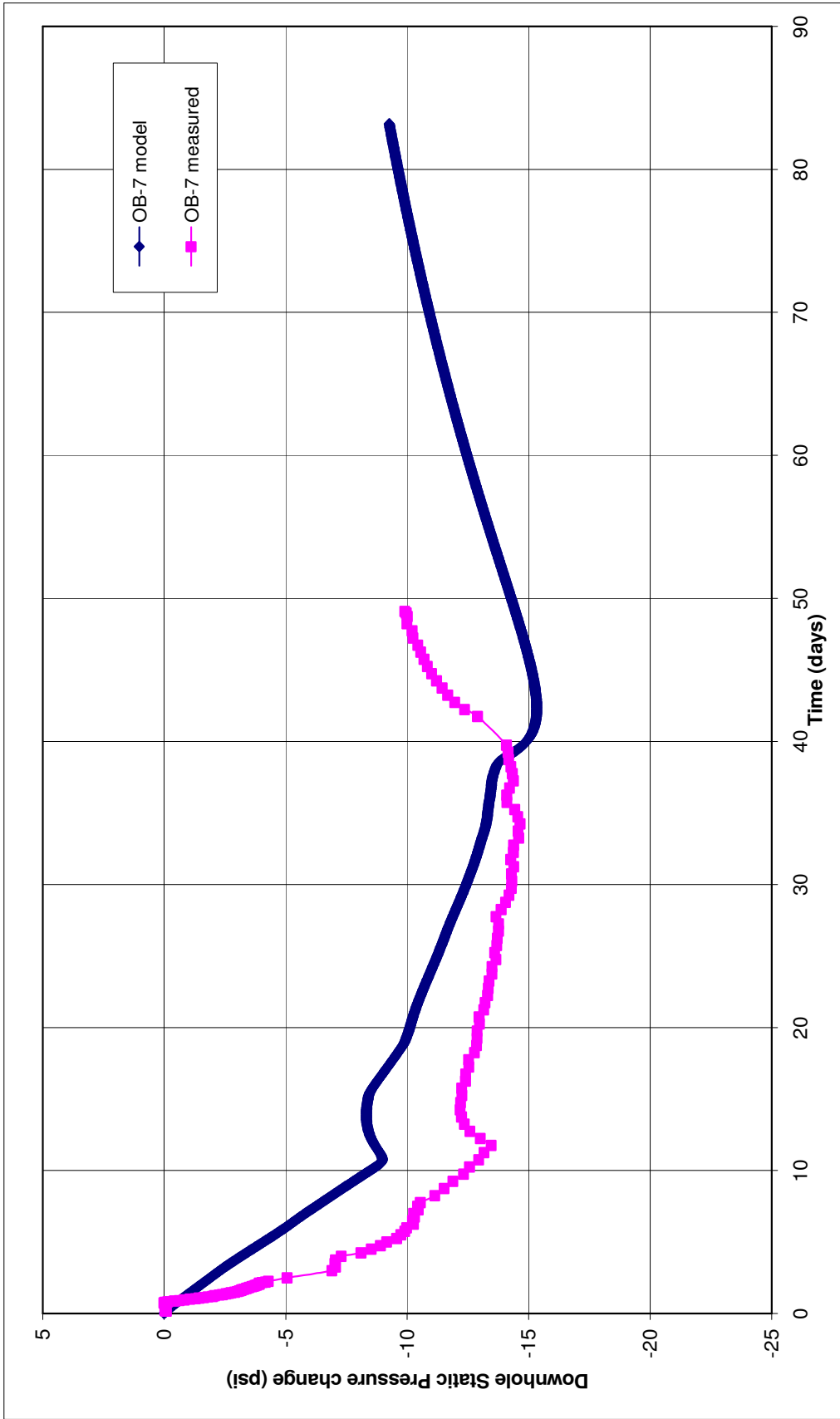


Figure 5.21 LTFT OB-7 Simulation Match

## 5.4 Forecasting

Five different development scenarios were carried out to predict the reservoir performance. The scenarios were performed with the assumption that flow rates are constant. With the exception of scenario 1, which is a depletion scenario, the development scenarios were run for a 30 year period. The injected fluid was assumed to have an enthalpy of 441 kJ/kg (105°C) and the mass ratio of injection to production was held at 0.8. The monitoring well OB-7 was used as representing the reservoir pressure in forecasting.

### 5.4.1 Scenario 1

This is a depletion case scenario with no injection into the reservoir. The forecast period was 10 years. The recently drilled Alangulu area wells were not included in this scenario.

Table 5.2 Details of production data of scenario 1

<b>Production wells</b>	<b>Flowrate (tph)</b>
OB-3	330
OB-5	300
OB-6	400
OB-8	320
OB-9	350
OB-10	410
OB-11	310
Total	2420

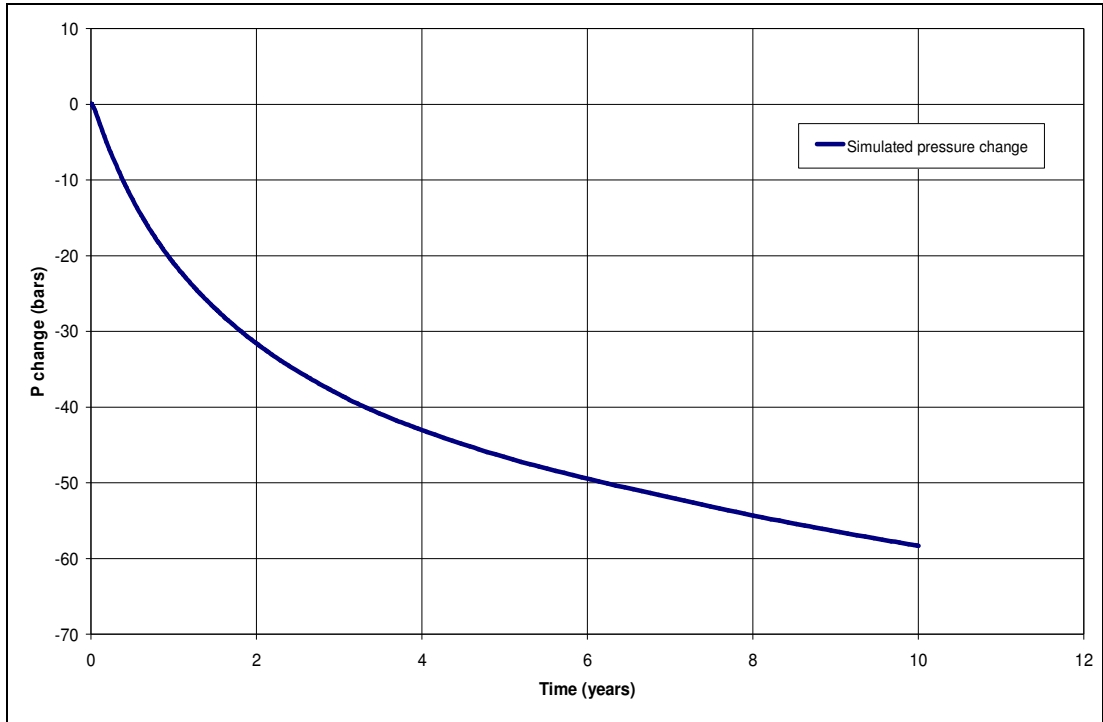


Figure 5.22 Simulated reservoir pressure change in scenario-1

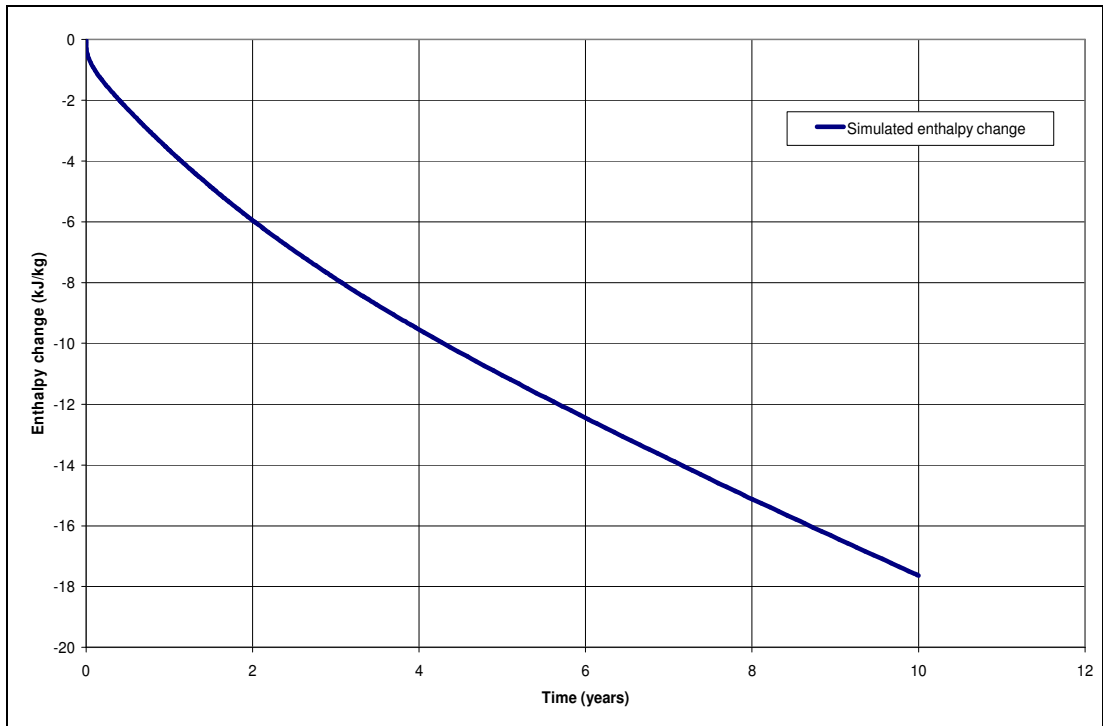


Figure 5.23 Simulated enthalpy change for well OB-3 in scenario-1

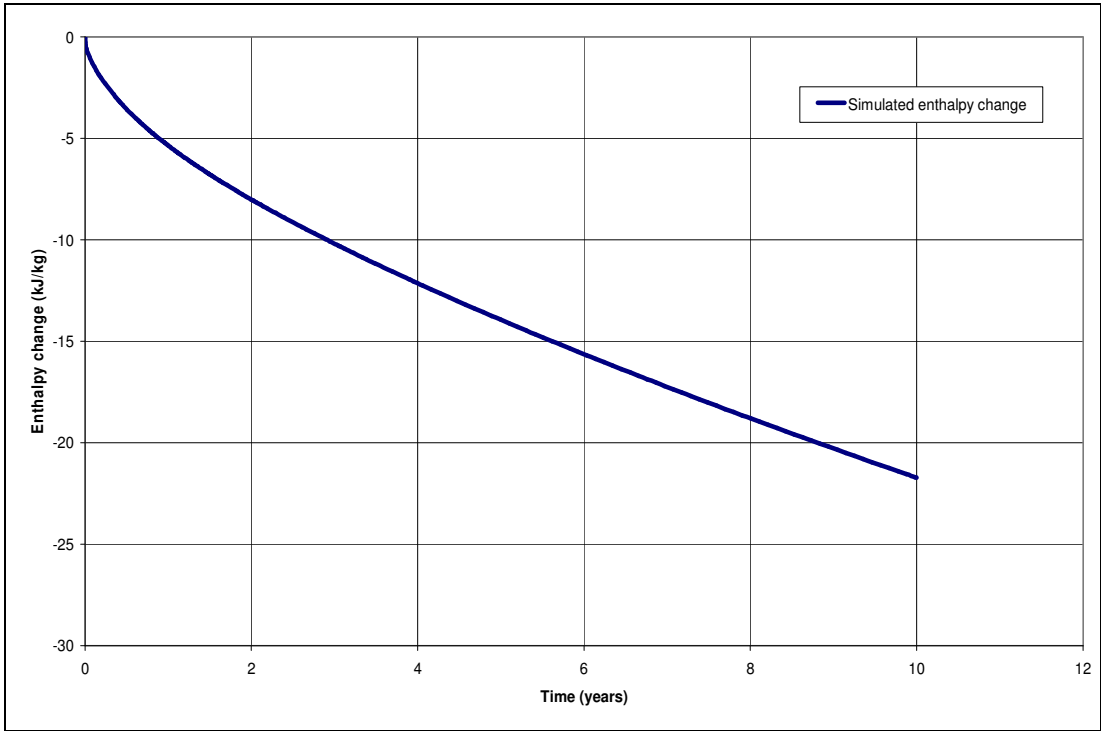


Figure 5.24 Simulated enthalpy change for well OB-5 in scenario-1

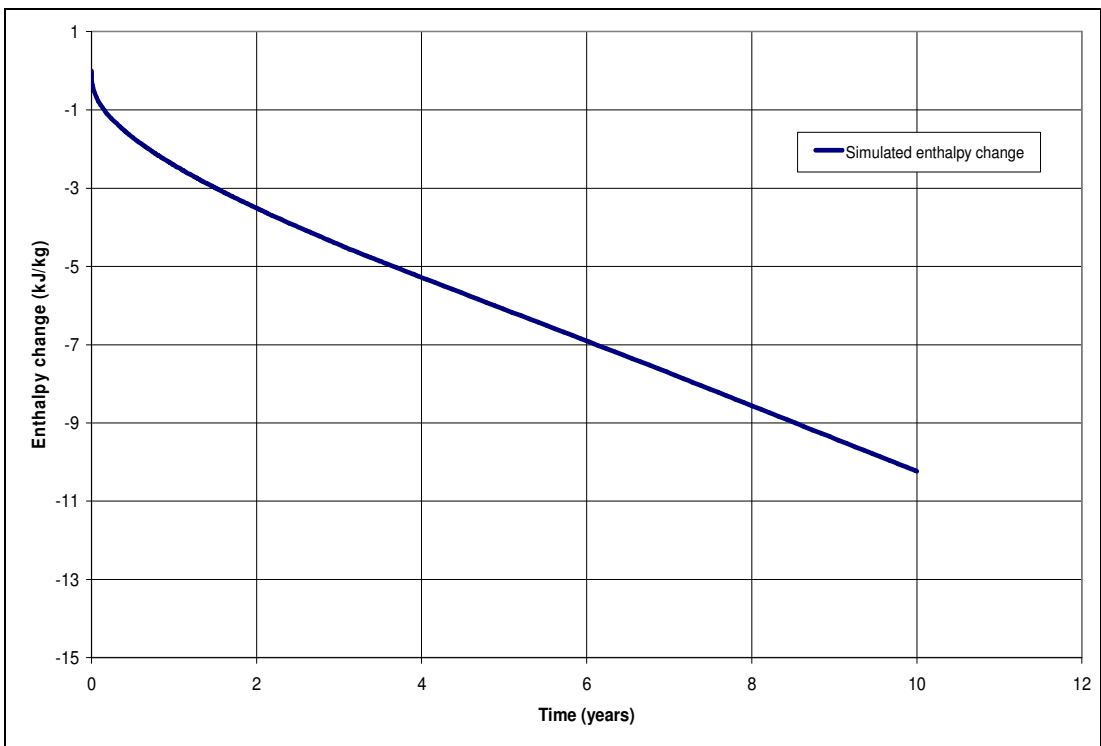


Figure 5.25 Simulated enthalpy change for well OB-9 in scenario-1

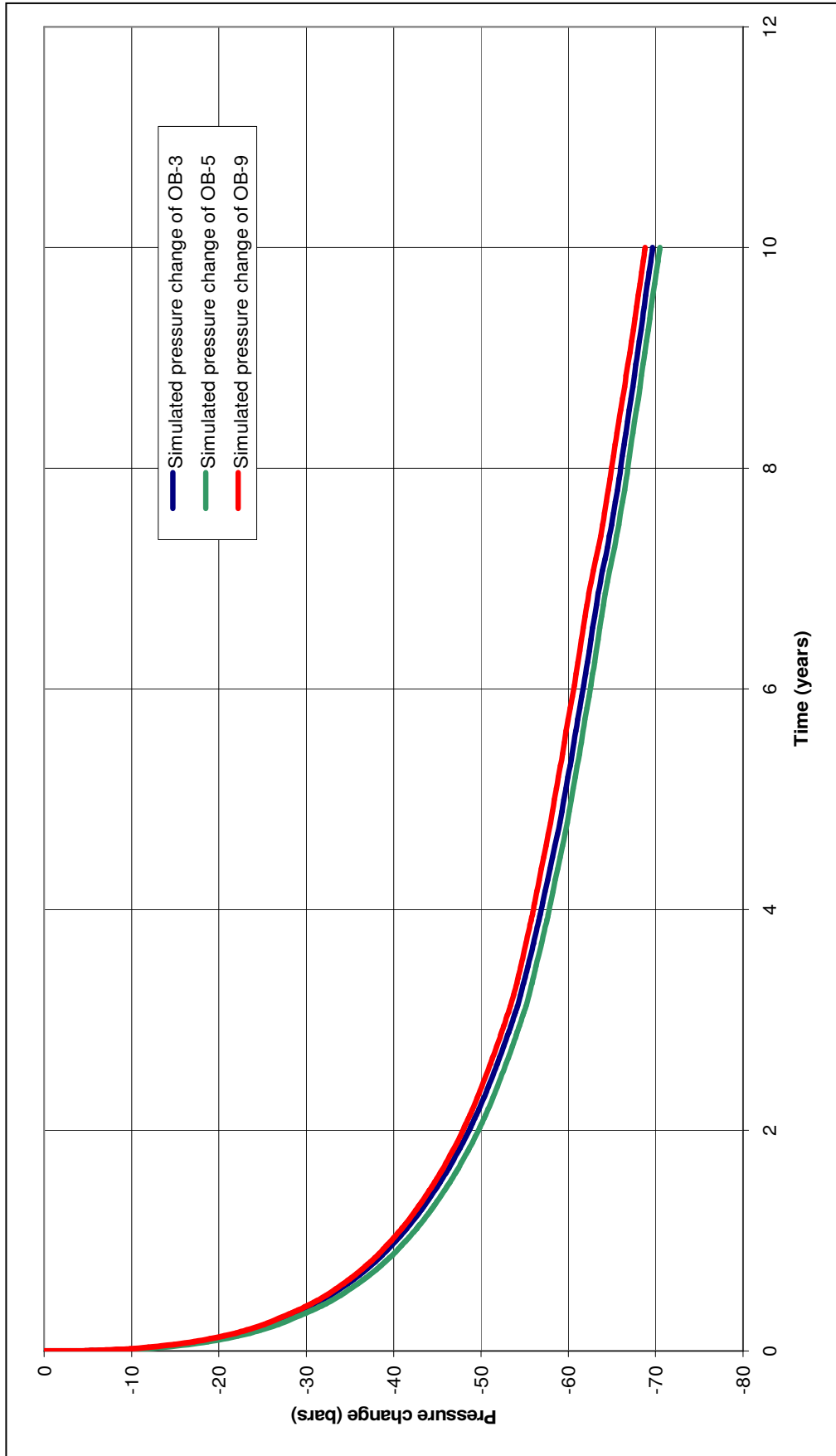


Figure 5.26 Simulated pressure change of production wells in scenario-1

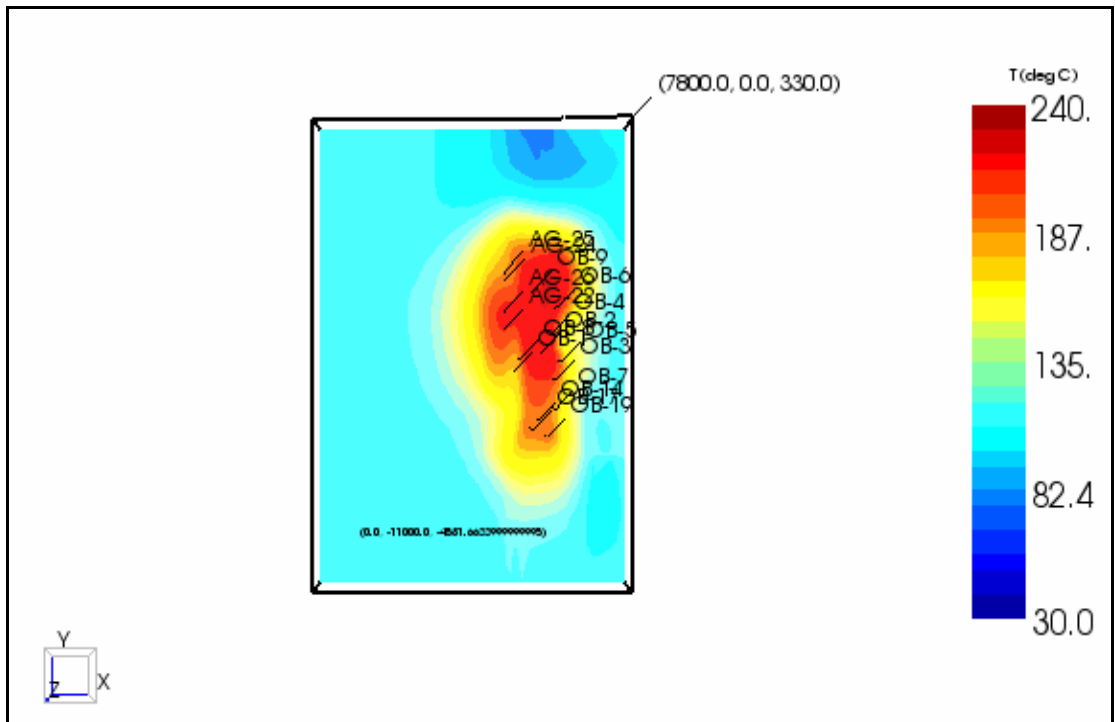


Figure 5.27 Initial state temperature distribution at main production horizon

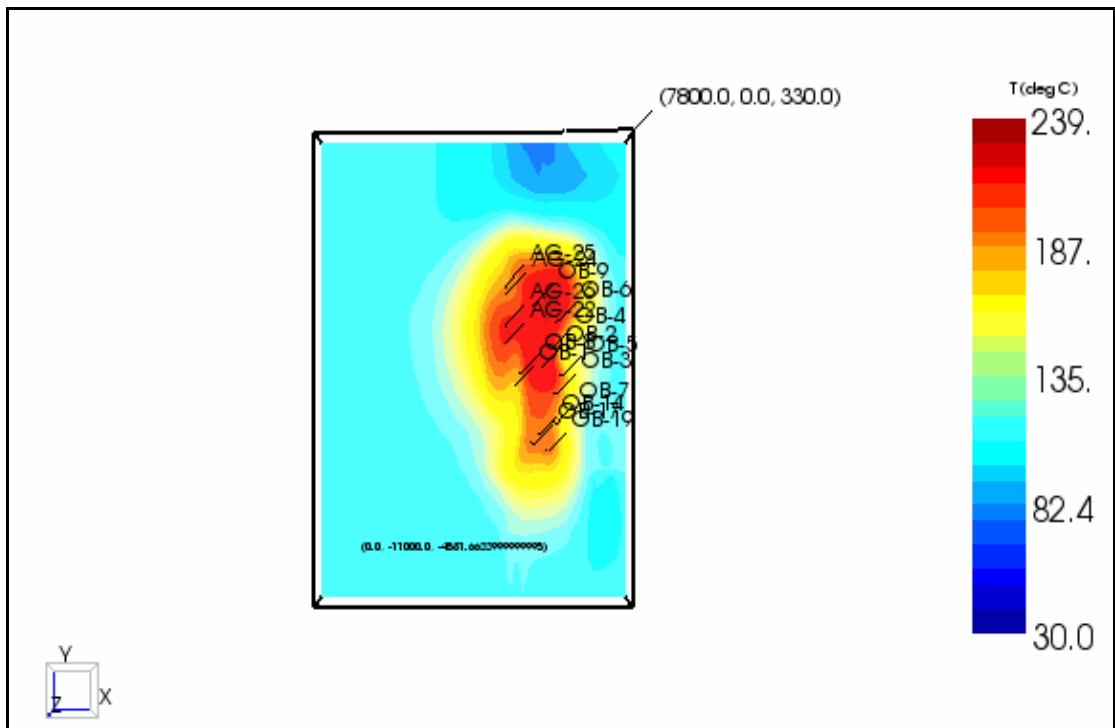


Figure 5.28 Final temperature distribution at main production horizon (-1300 m msl) in scenario-1

## 5.4.2 Scenario 2

Table 5.3 Details of production/injection data in scenario-2

Production wells	Flowrate (tph)	Injection wells	Flowrate (tph)
OB-3	330	OB-14	660
OB-5	300	OB-17	660
OB-6	400	OB-19	680
OB-8	400		
OB-9	350		
OB-10	410		
OB-11	310		
Total	2500	Total	2000

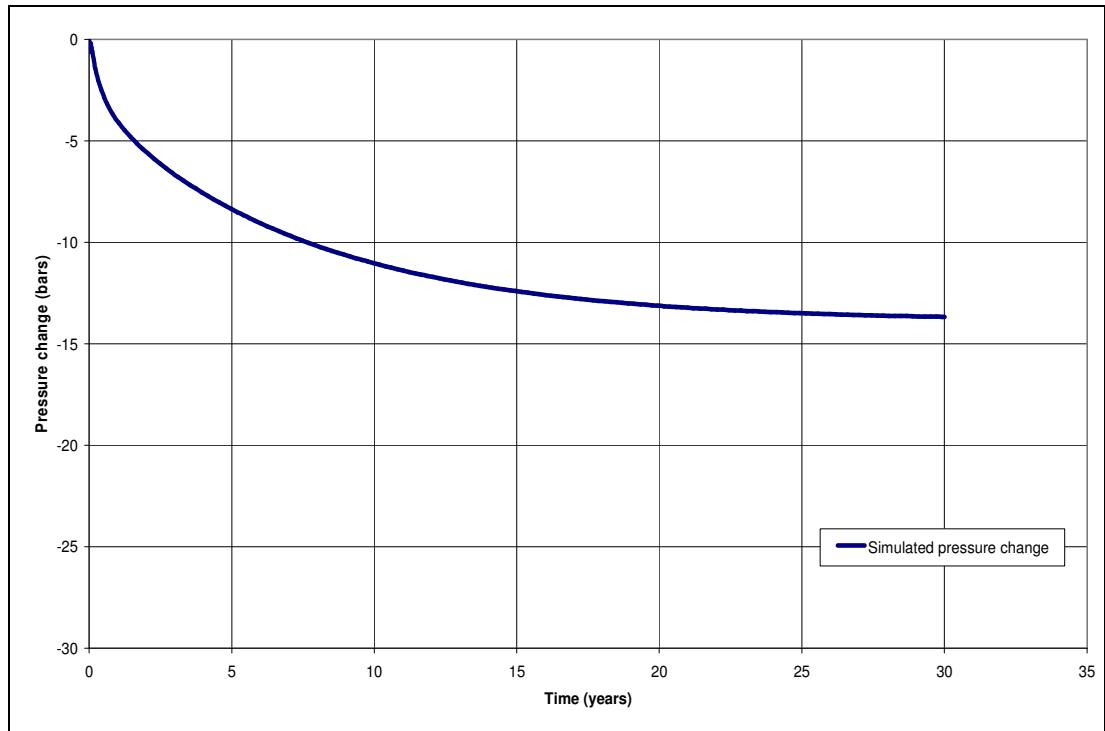


Figure 5.29 Simulated reservoir pressure change in scenario-2

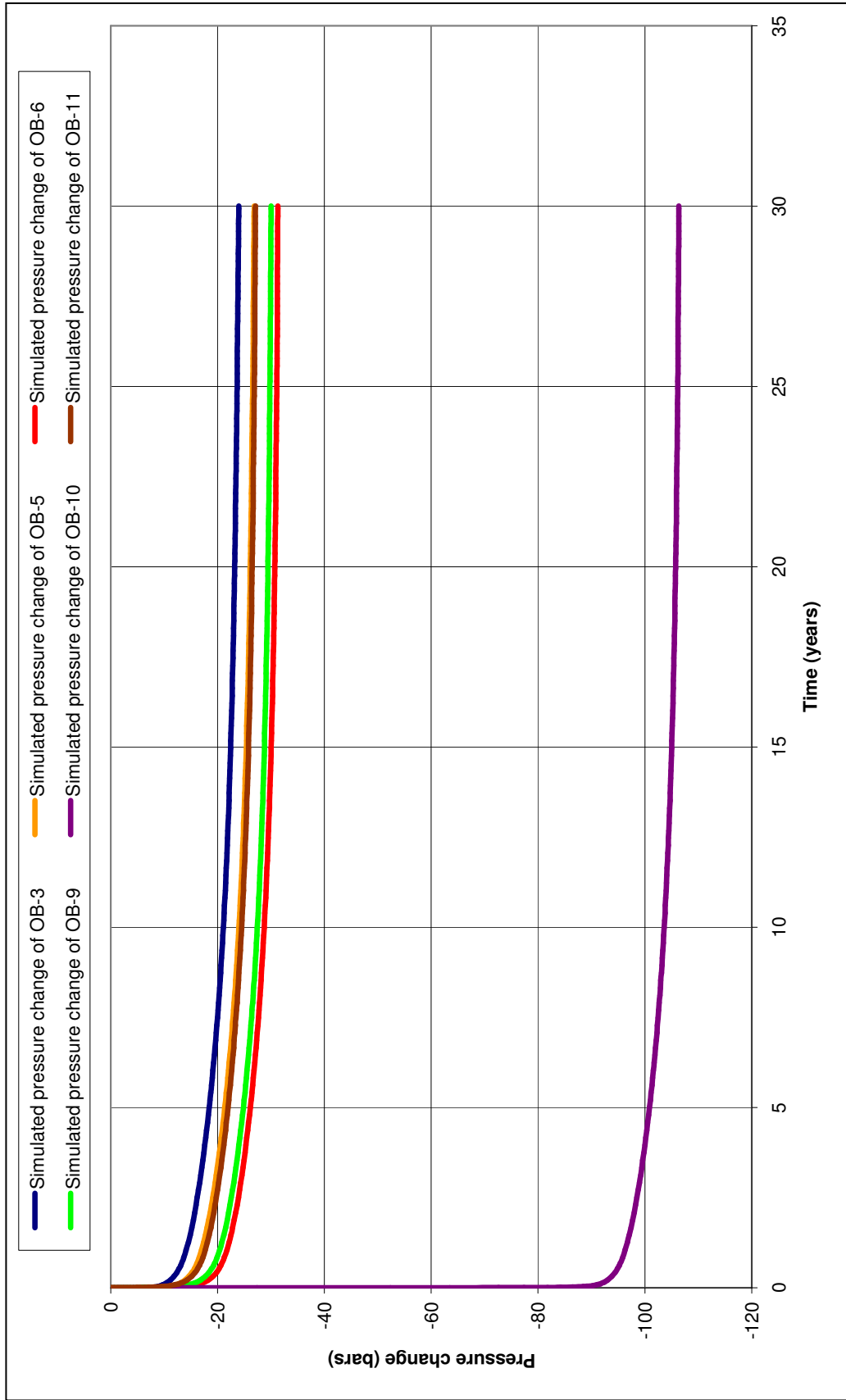


Figure 5.30 Simulated pressure change of production wells in scenario-2

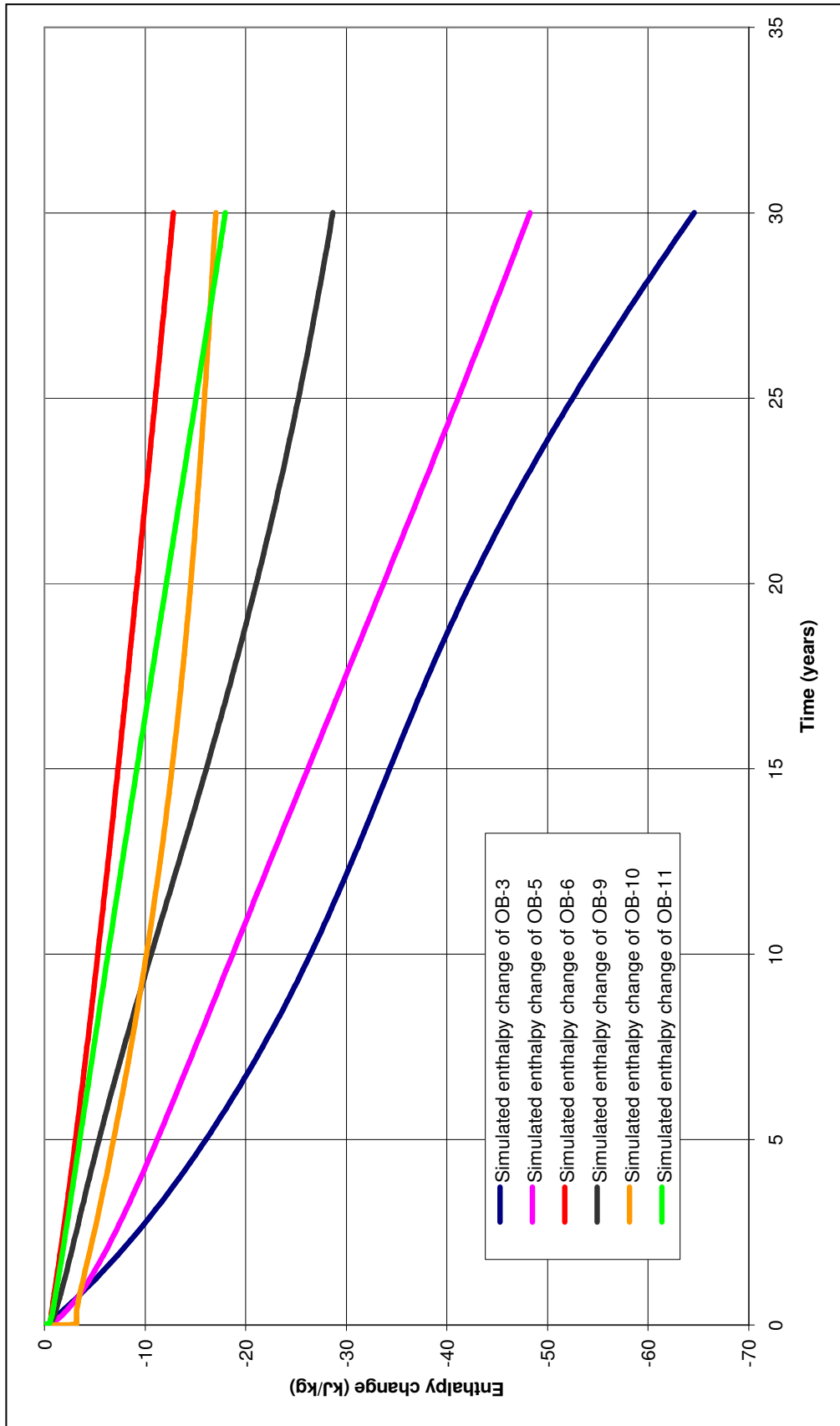


Figure 5.31 Simulated enthalpy change of production wells in scenario-2

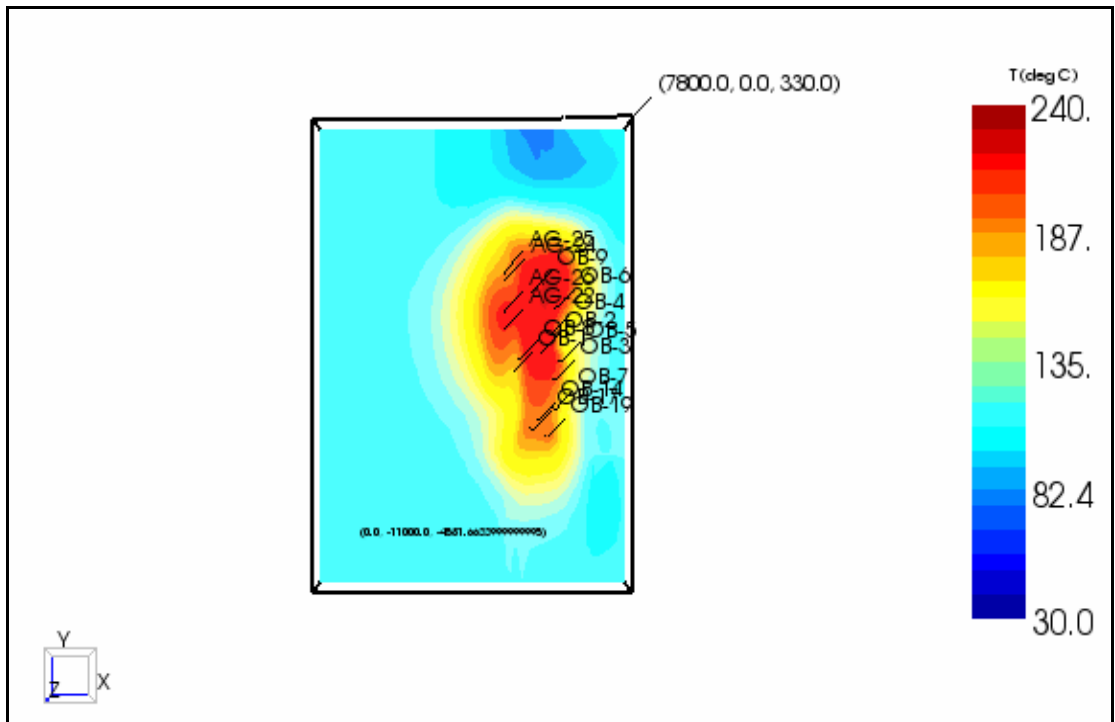


Figure 5.32 Initial temperature distribution at main production horizon (-1300msl)

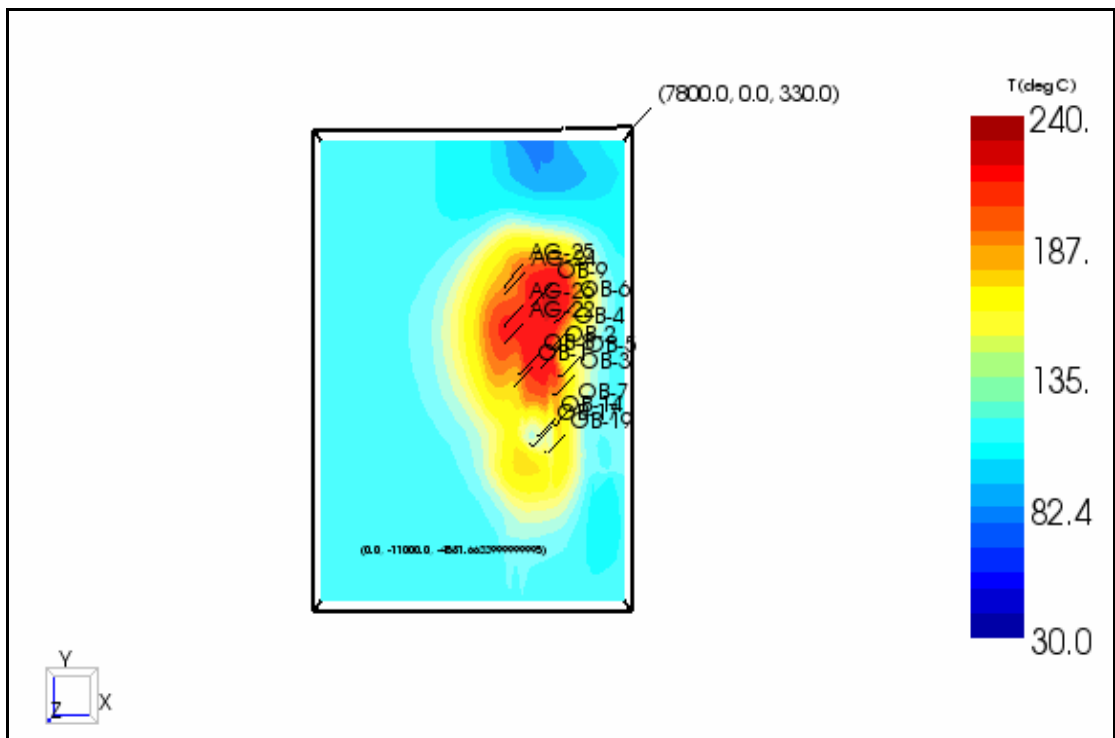


Figure 5.33 Final temperature distribution at main production horizon (-1300m msl) in scenario-2

### 5.4.3 Scenario 3

Table 5.4 Details of production/injection data in scenario 3

Production wells	Flowrate (tph)	Injection wells	Flowrate (tph)
OB-5	300	OB-3	75
OB-6	400	OB-9	350
OB-10	410	AG-22	440
OB-11	310	AG-24	500
OB-14	680	AG-25	500
OB-17	420	AG-26	150
Toatal	2520	Total	2015

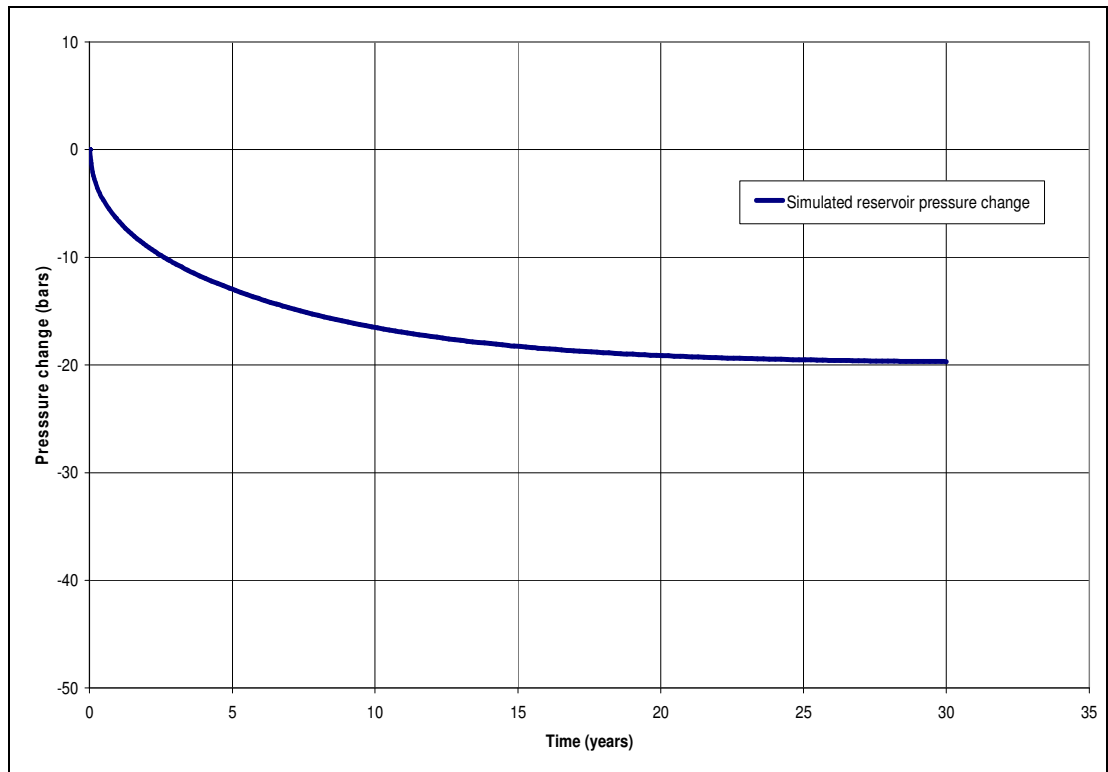


Figure 5.34 Simulated reservoir pressure change in scenario-3

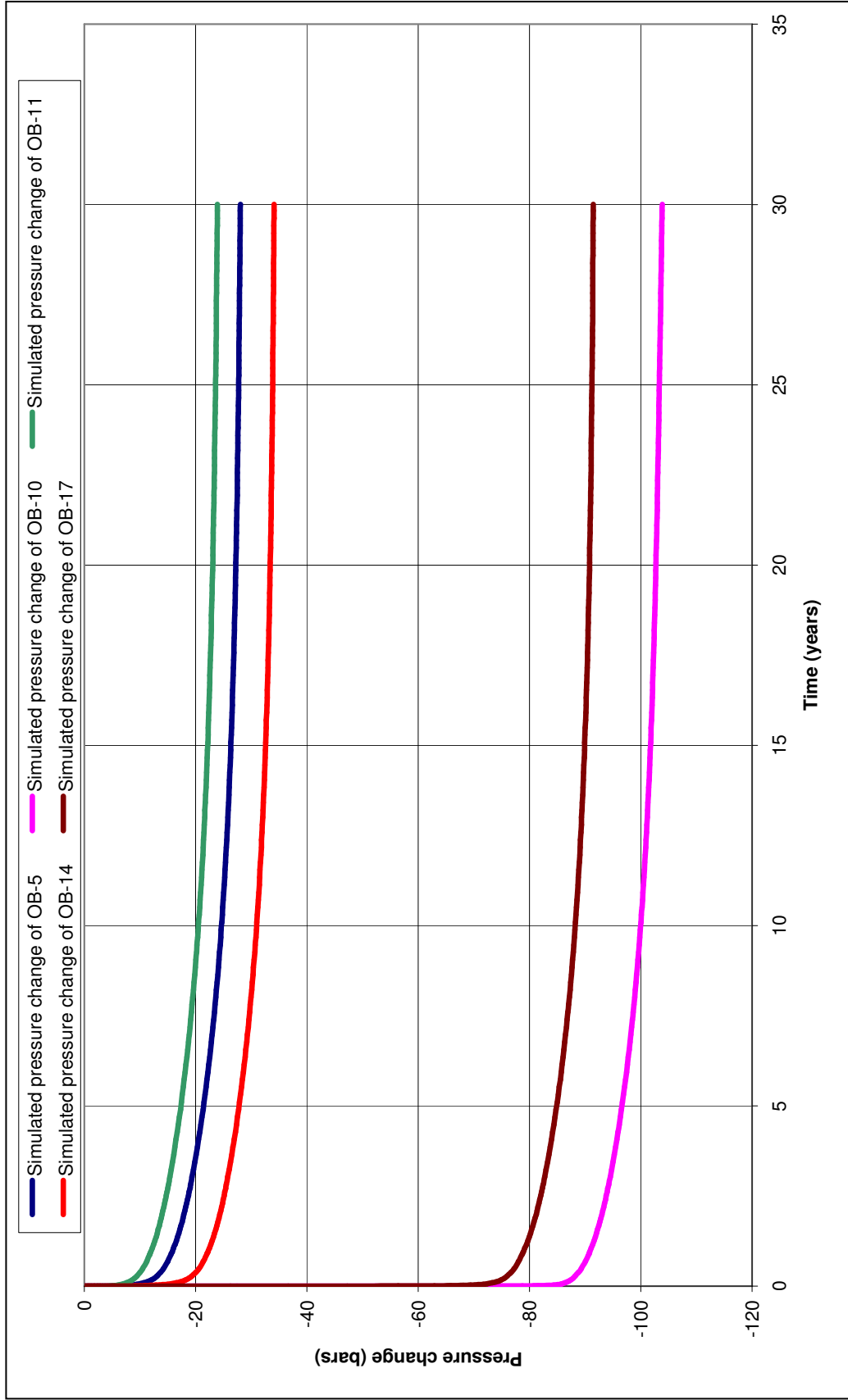


Figure 5.35 Simulated pressure change of production wells in scenario-3

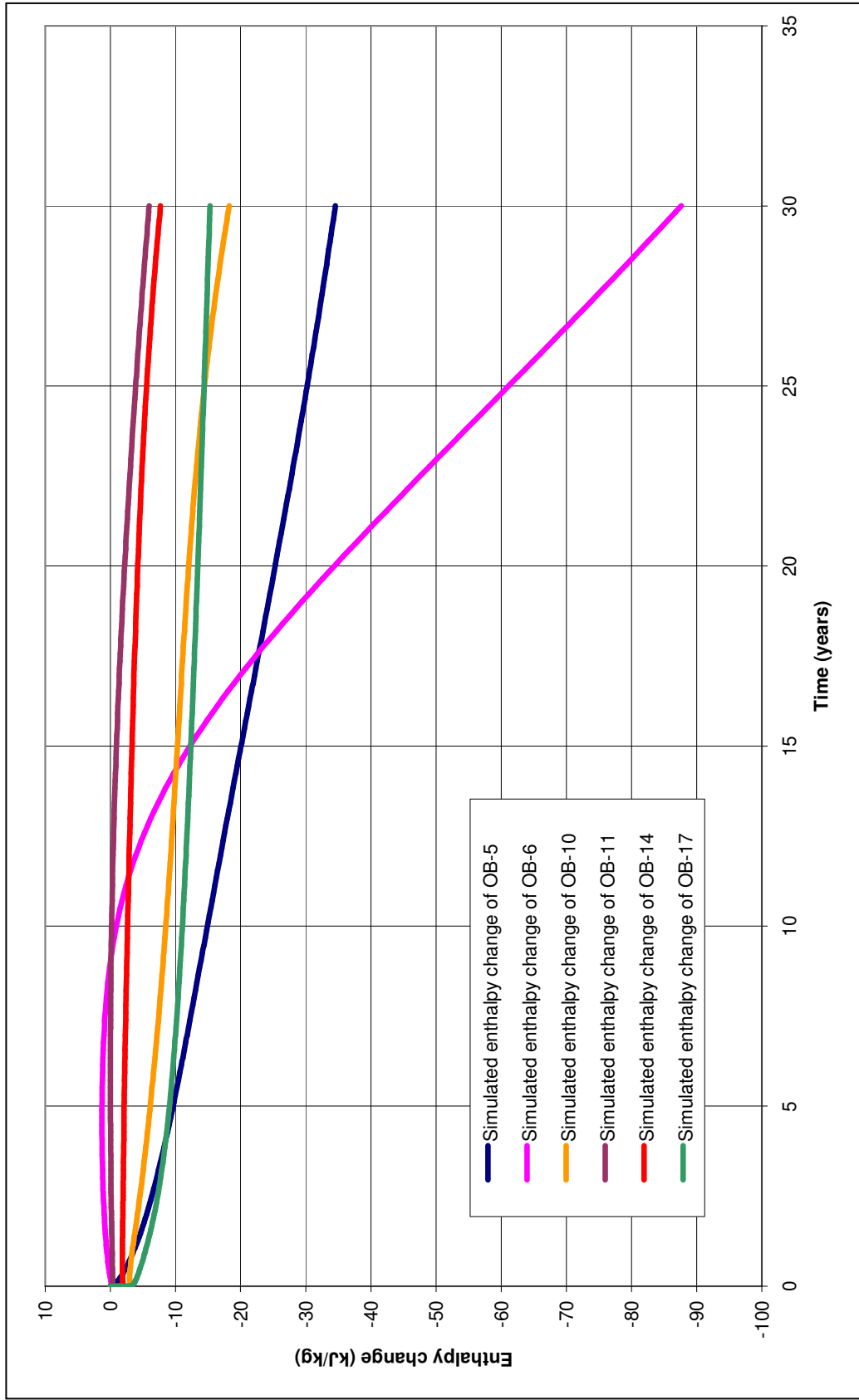


Figure 5.36 Simulated enthalpy change of production wells in scenario-3

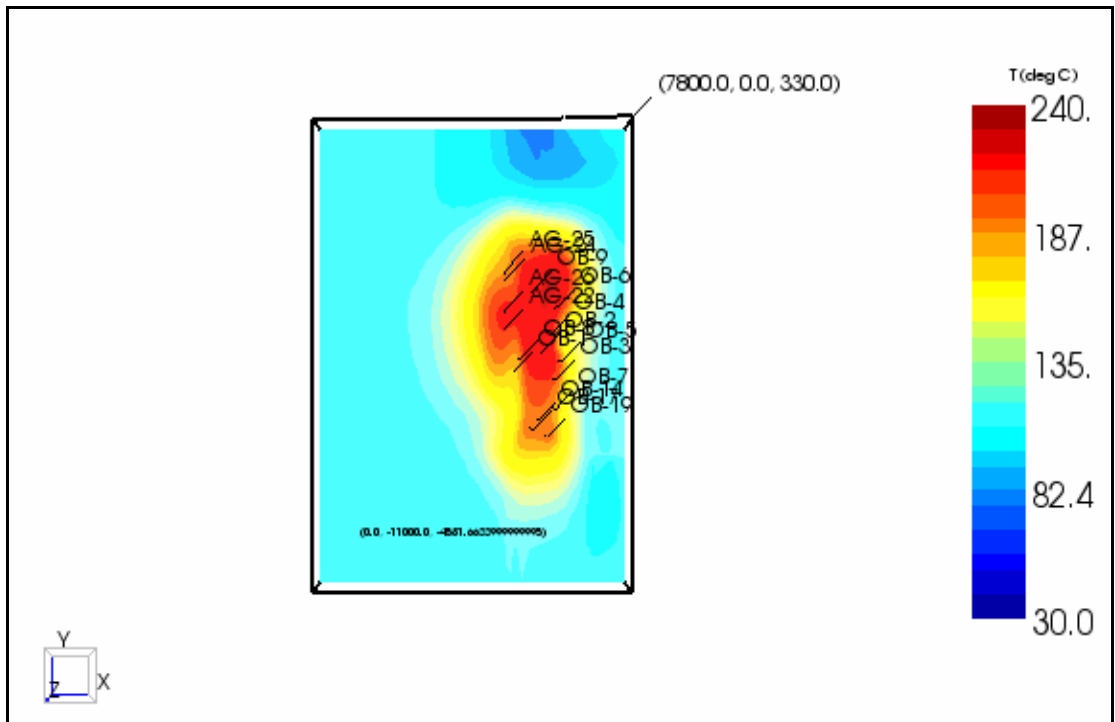


Figure 5.37 Initial temperature distribution at main production horizon (-1300msl)

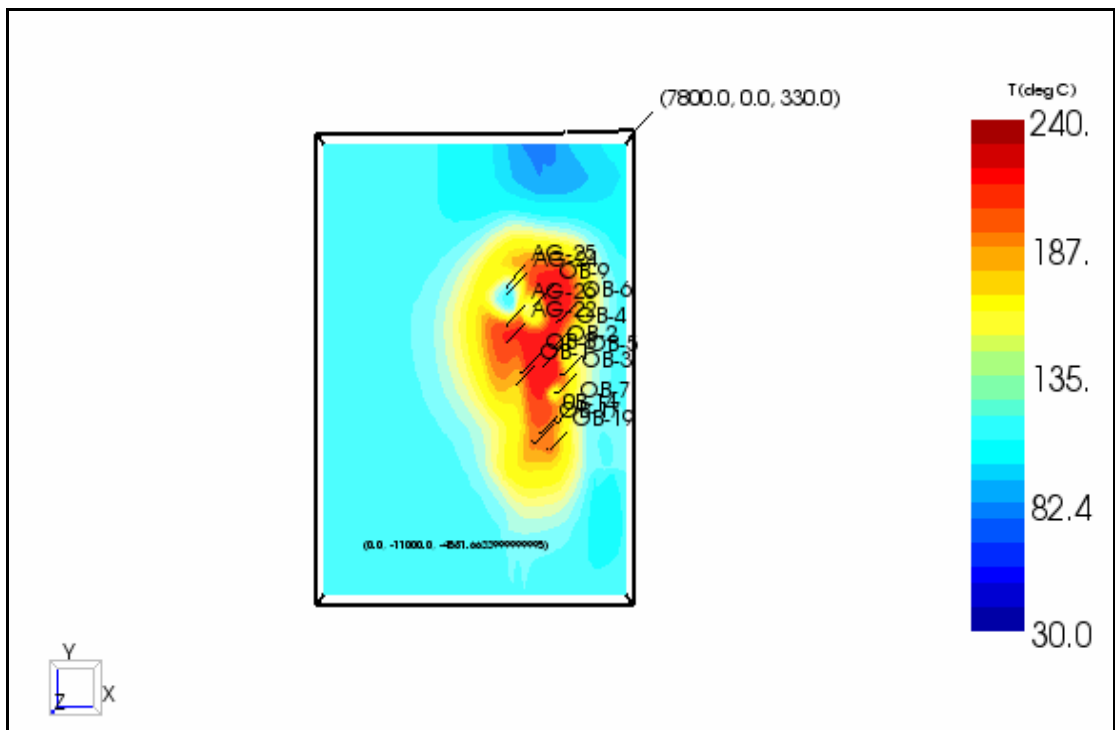


Figure 5.38 Final temperature distribution at main production horizon (-1300msl) in scenario-3

#### 5.4.4 Scenario 4

Table 5.5 Details of production/injection data in scenario 4

Production wells	Flowrate (tph)	Injection wells	Flowrate (tph)
OB-5	300	OB-3	75
OB-6	400	OB-8	300
OB-10	410	OB-9	350
OB-11	310	AG-22	340
OB-14	680	AG-24	400
OB-17	420	AG-25	400
		AG-26	150
Toatal	2520	Total	2015

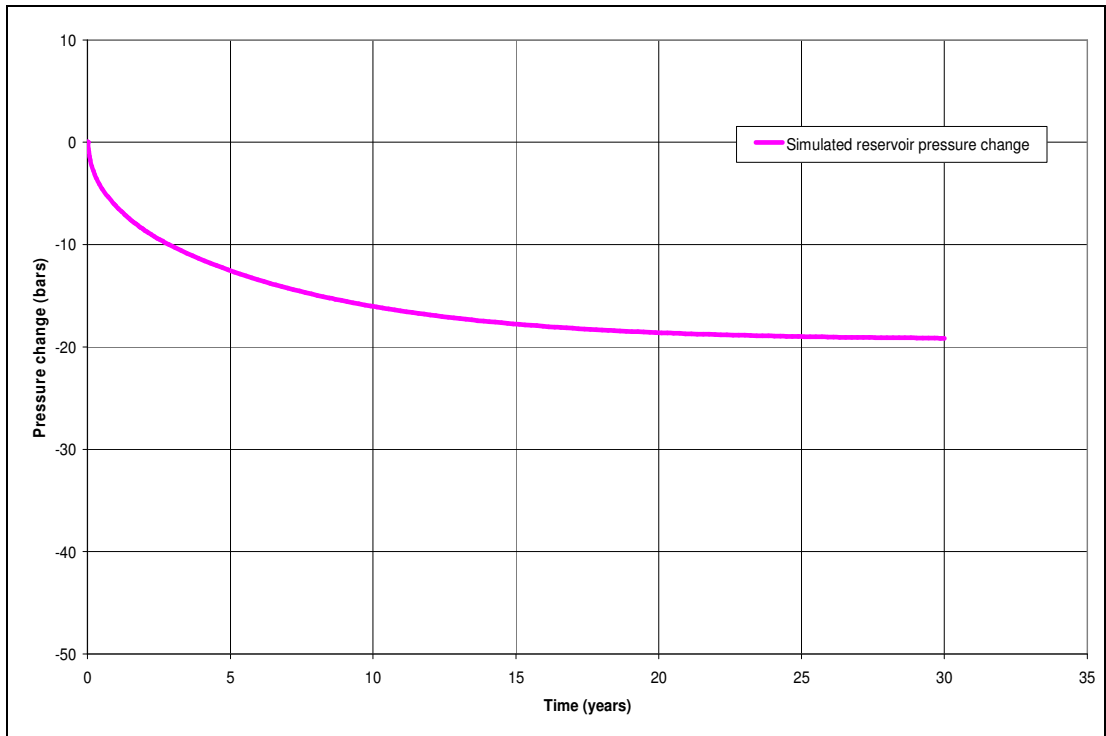


Figure 5.39 Simulated reservoir pressure change in scenario-4

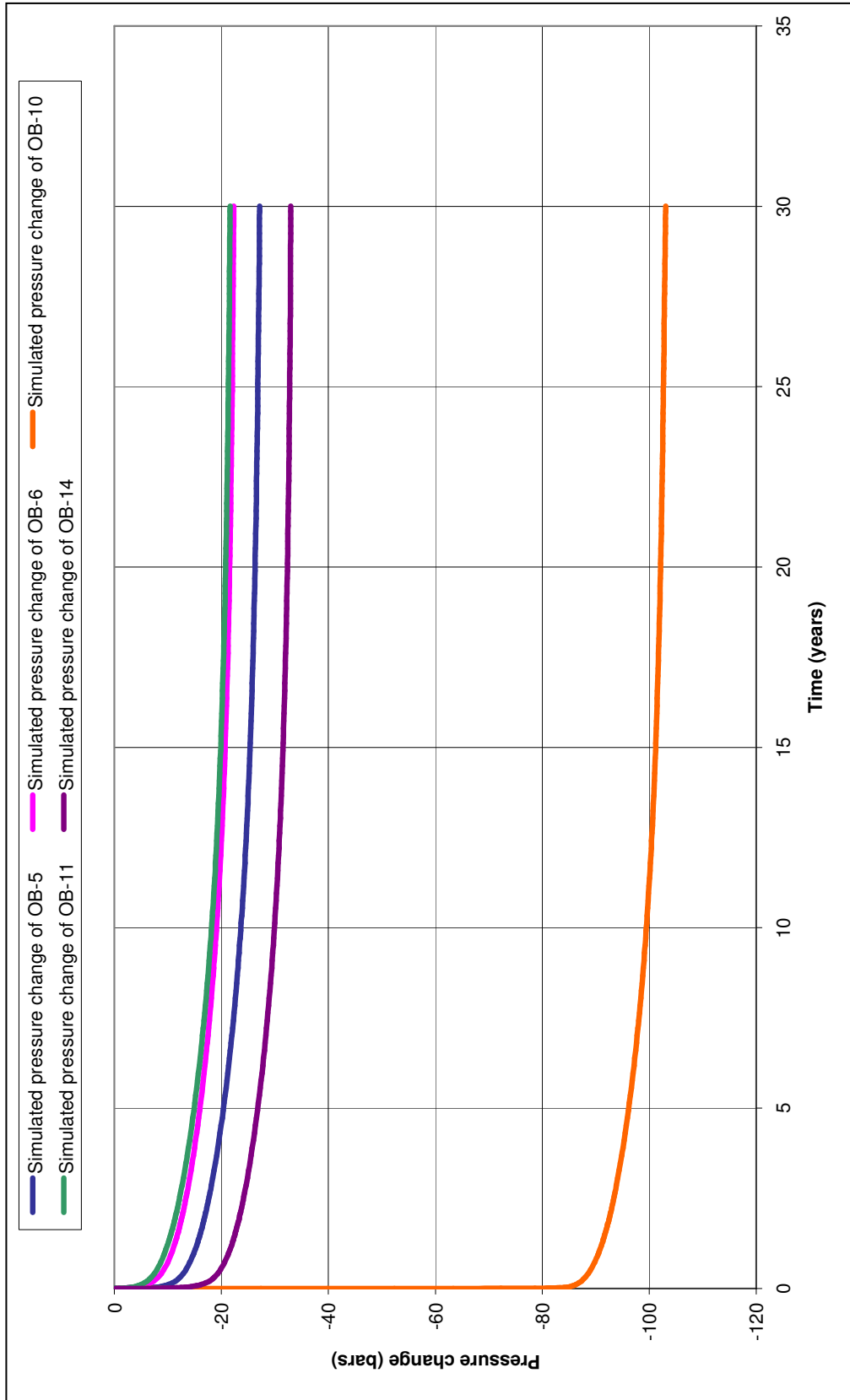


Figure 5.40 Simulated pressure change of production wells in scenario-4

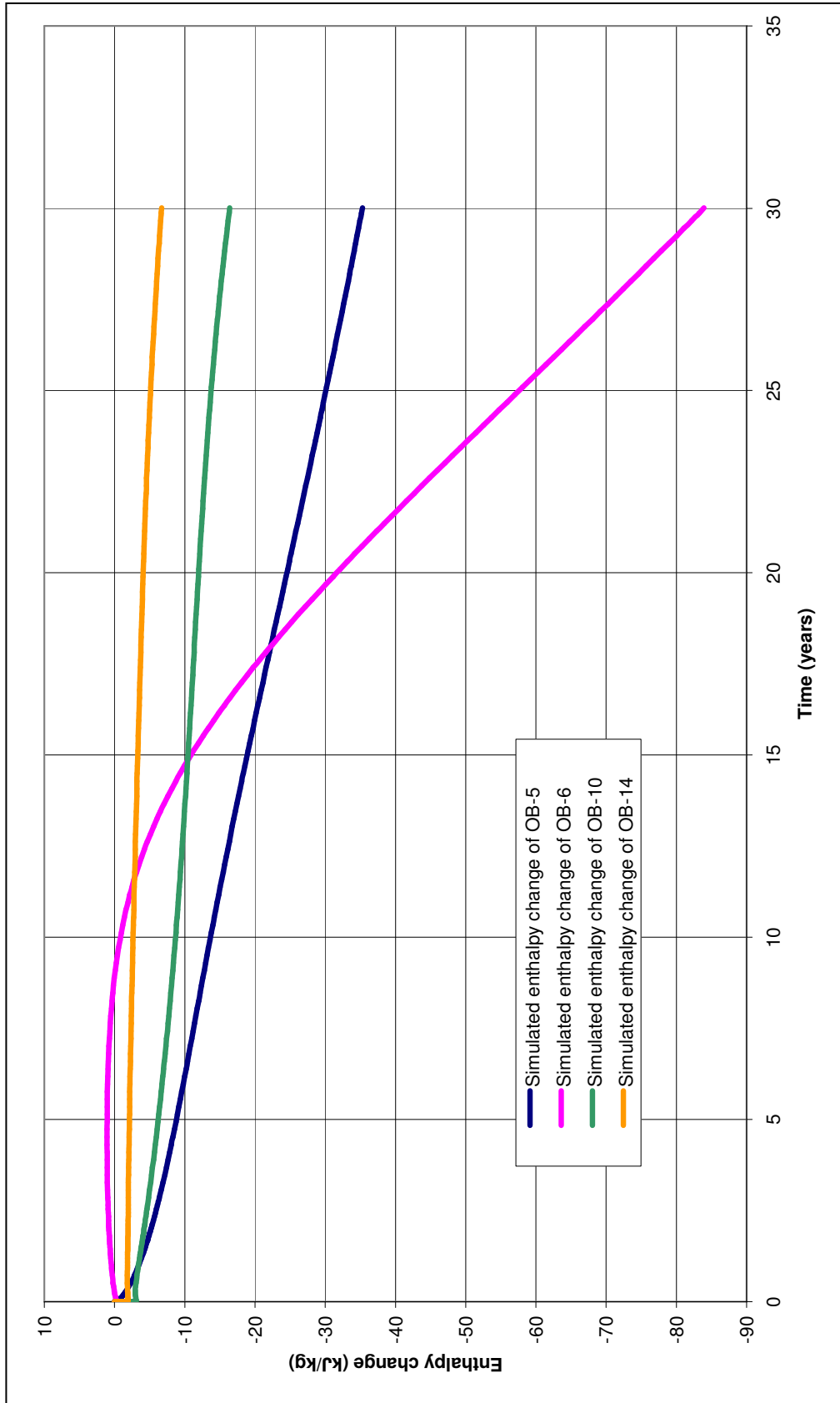


Figure 5.41 Simulated enthalpy change of production wells in scenario-4

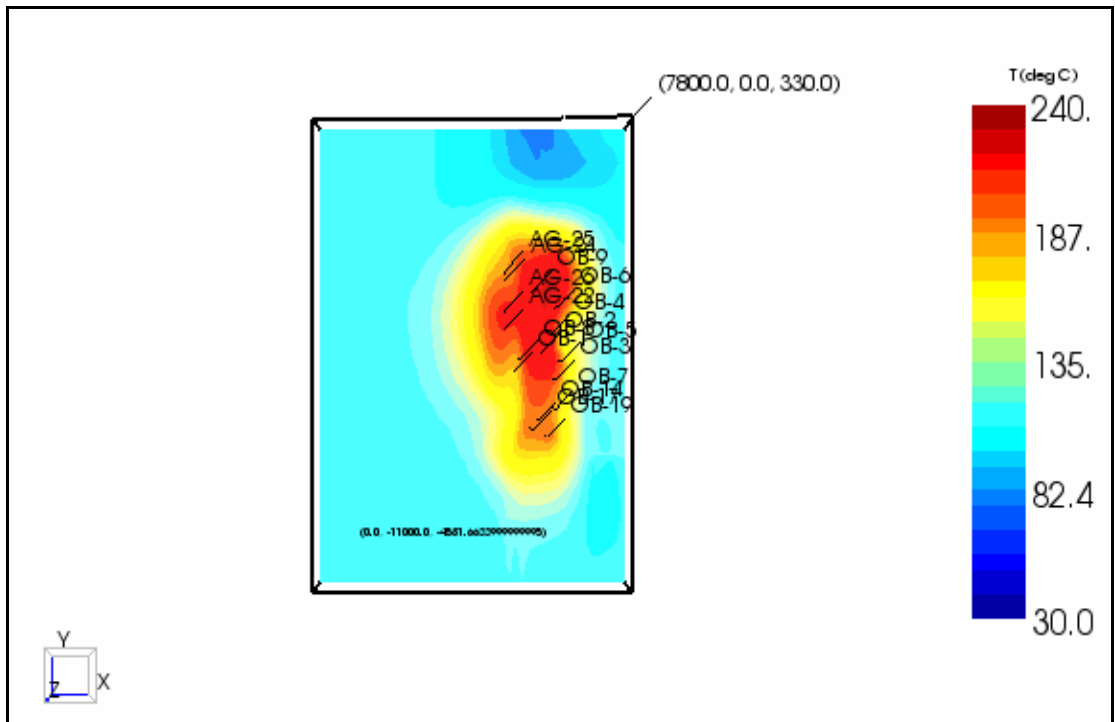


Figure 5.42 Initial temperature distribution at main production horizon (-1300msl)

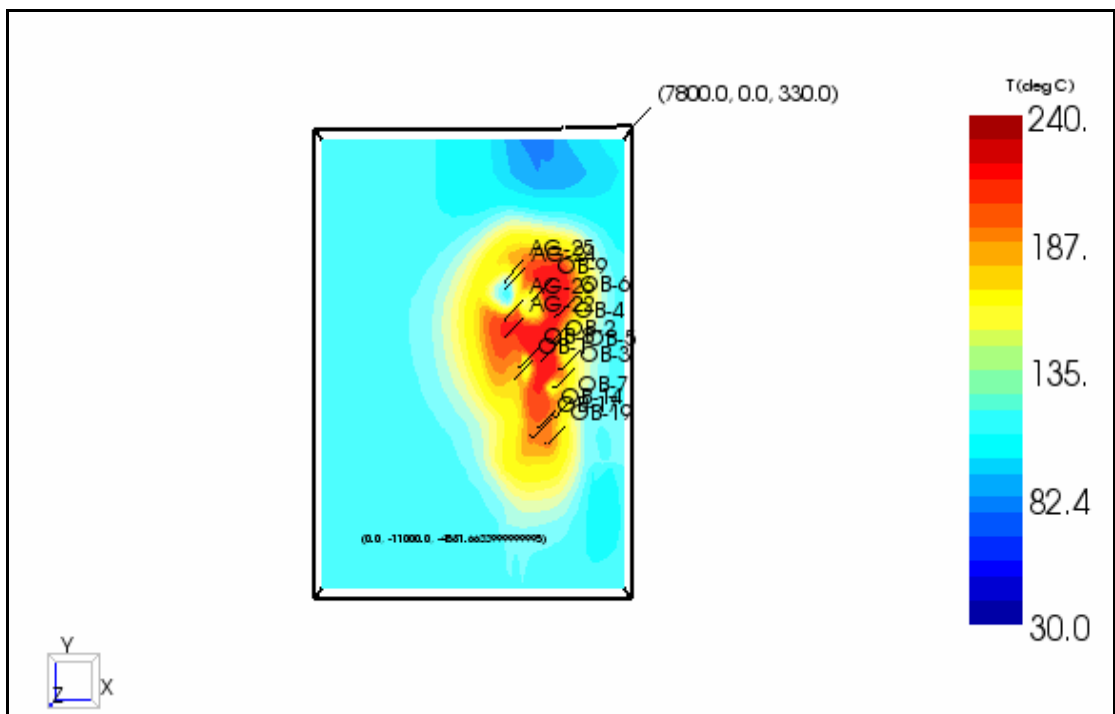


Figure 5.43 Final temperature distribution at main production horizon (-1300msl) in scenario-4

### 5.4.5 Scenario 5

Table 5.6 Details of production/injection data in scenario 5

Production wells	Flowrate (tph)	Injection wells	Flowrate (tph)
OB-5	300	OB-3	75
OB-6	400	OB-8	0
OB-10	410	OB-9	0
OB-11	310	AG-22	440
OB-14	680	AG-24	500
OB-17	420	AG-25	500
		AG-26	500
Toatal	2520	Total	2015

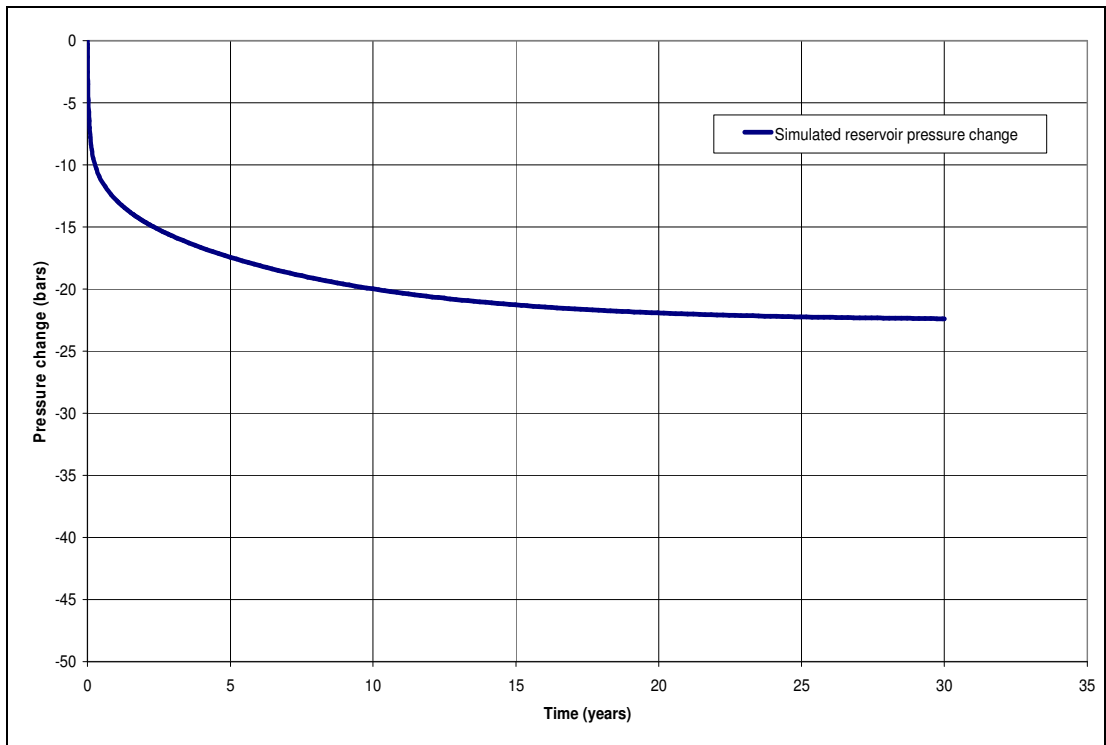


Figure 5.44 Simulated reservoir pressure change in scenario-5

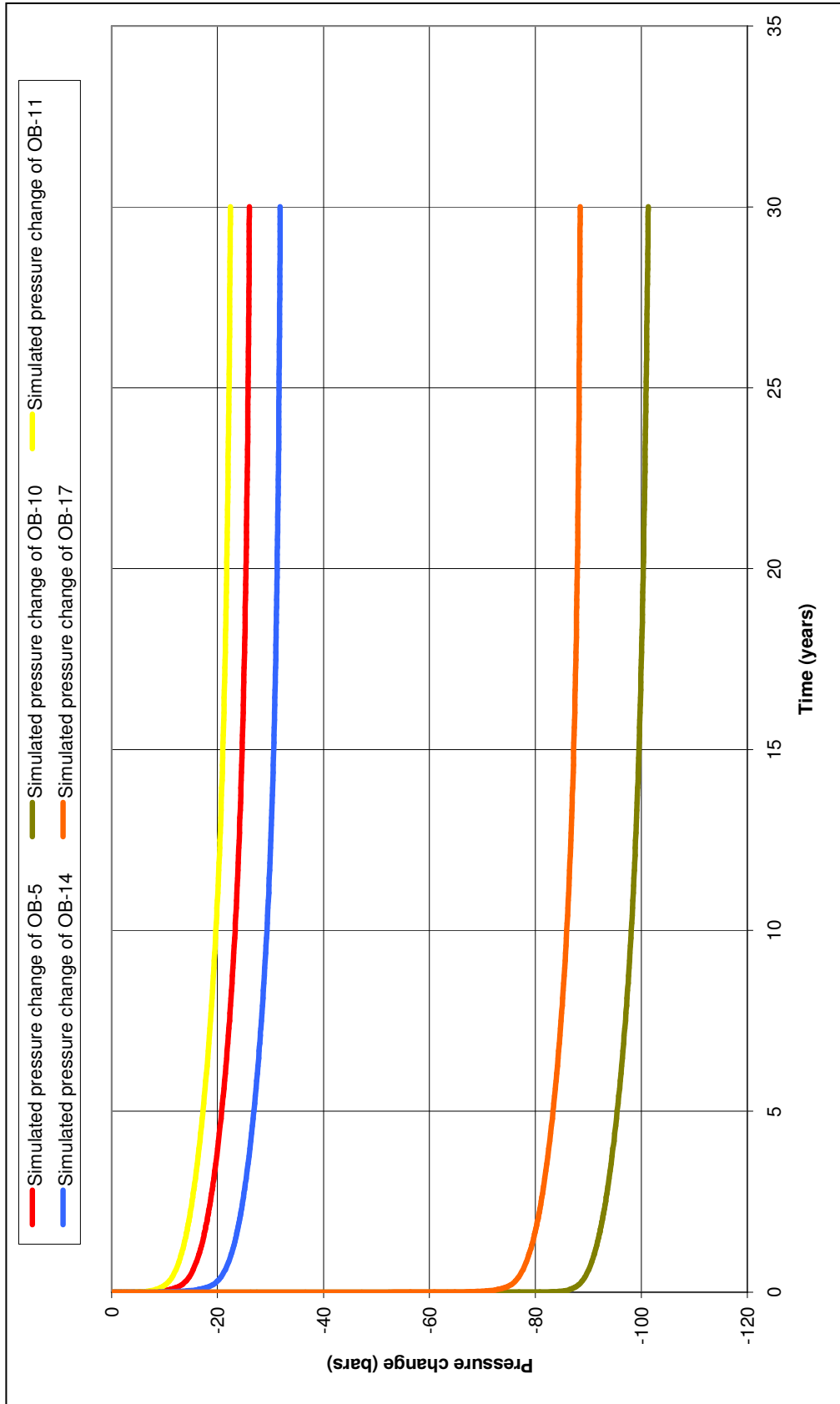


Figure 5.45 Simulated pressure change of production wells in scenario-5

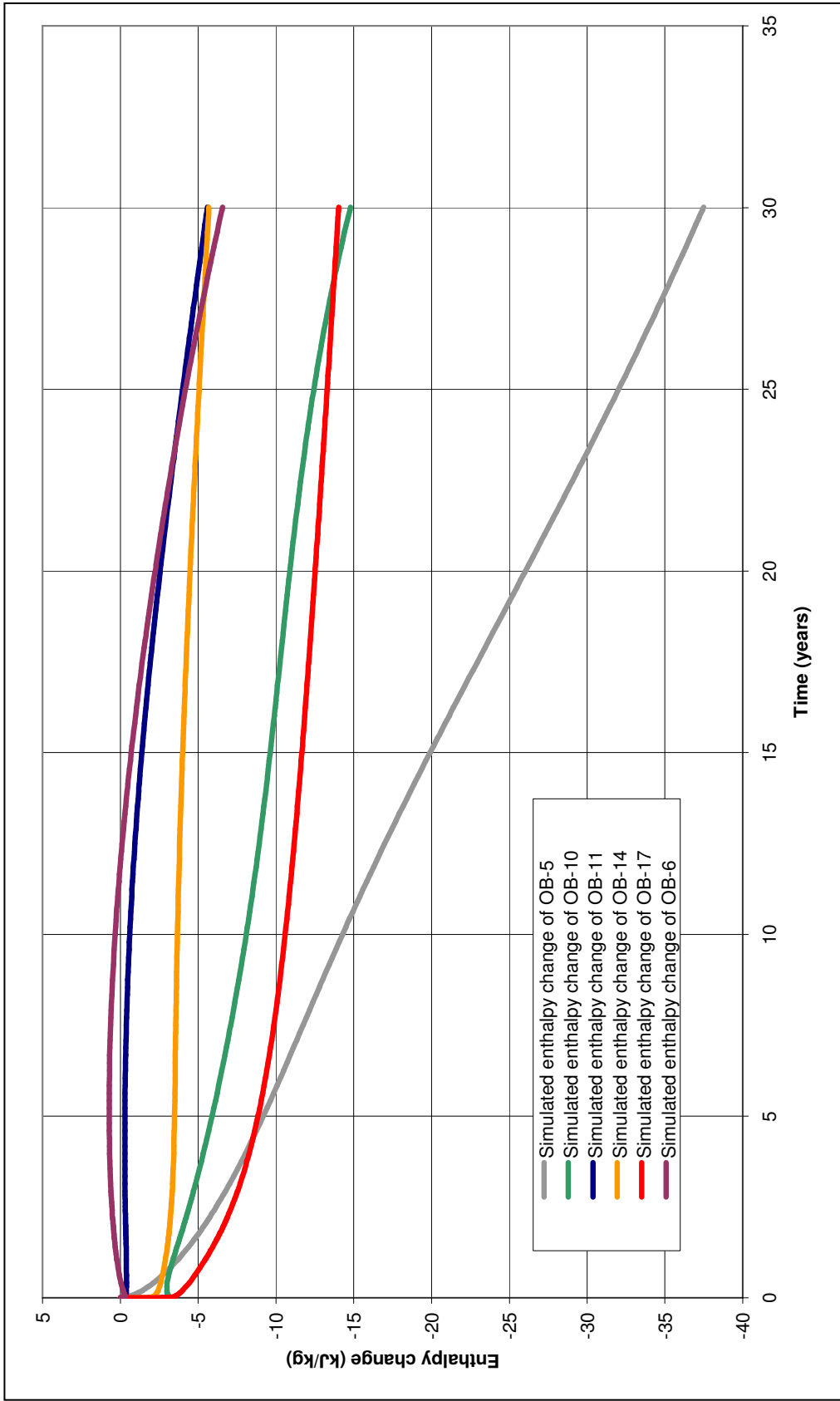


Figure 5.46 Simulated enthalpy change of production wells in scenario-5

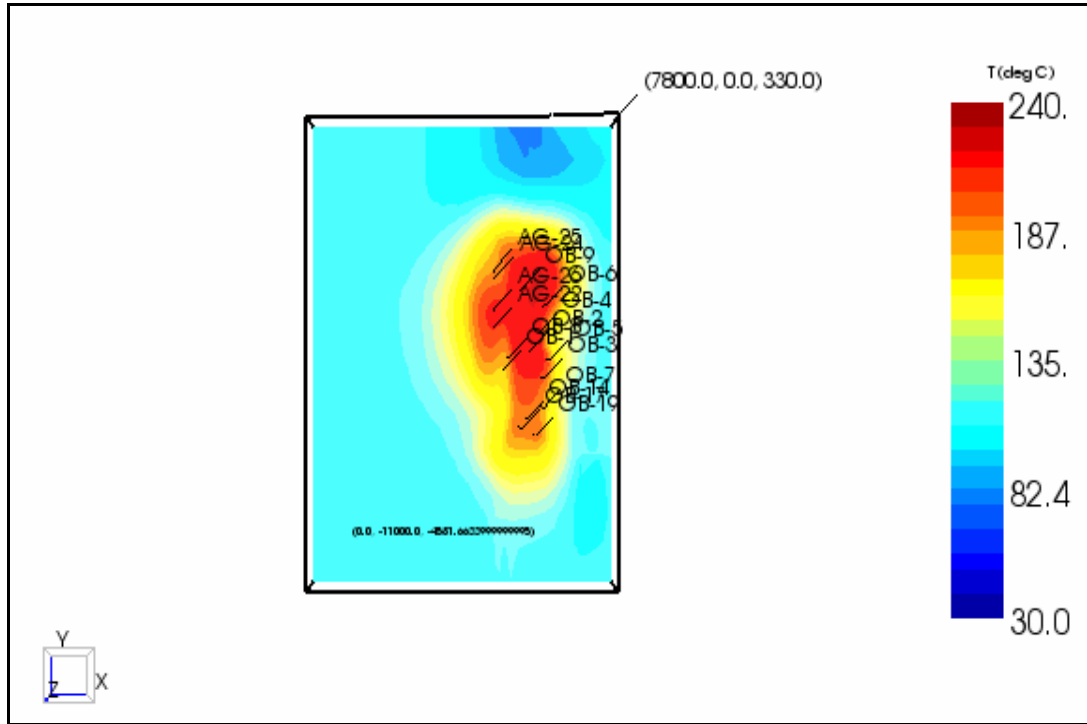


Figure 5.47 Initial temperature distribution at main production horizon (-1300msl)

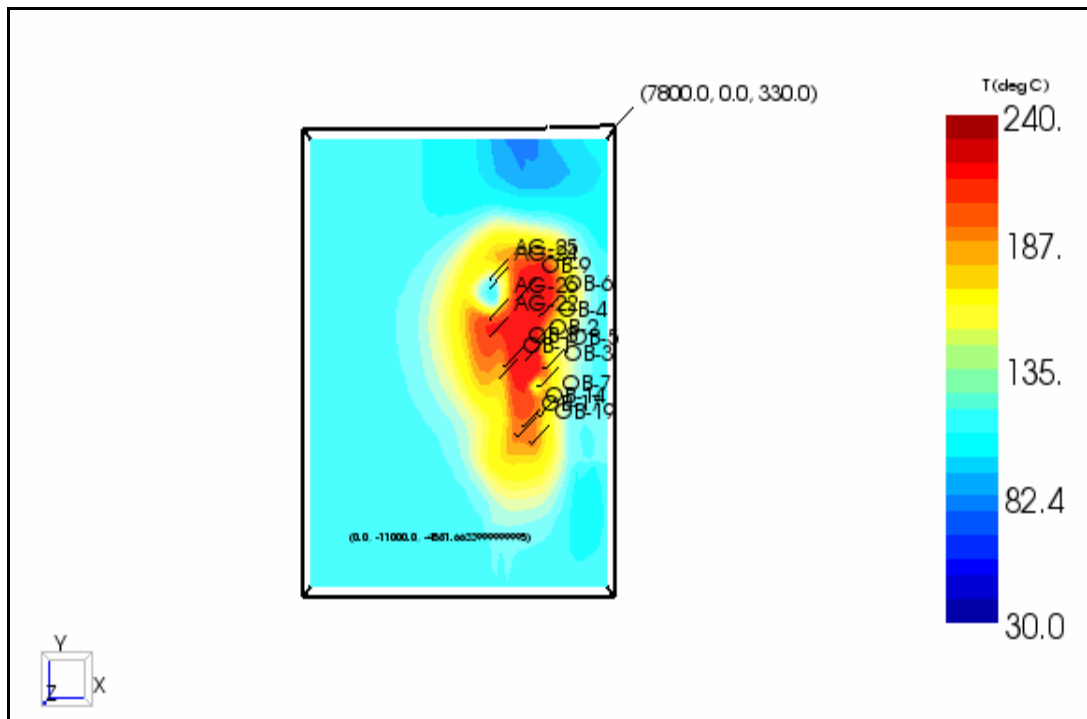


Figure 5.48 Final temperature distribution at main production horizon (-1300msl) in scenario-5

## 5.5 Discussion

The reservoir permeability and connectivity is quite high and is continuous throughout the reservoir as seen with the rapid pressure response to production and injection during the LTFT and forecasting runs.

The model forecasts show that the reservoir pressure declines almost equally in all areas of the reservoir and is in proportion to the net withdrawal of fluid. The pressure decline suggests that injection will be critical to support reservoir pressure and maintain productivity, regardless of the location of injection.

The first forecast run is a depletion case scenario; the reservoir was produced from wells located in the center of the field for a 10 year period. The recently drilled wells in the Alangulu area were not included in this prediction run. The reservoir pressure shows a rapid decline of 31 bars in the first couple of years and continues to drop to 58 bars after ten years. The production wells suffer a continuous steady decline in enthalpy reaching 22 kJ/kg in well OB-5.

In the second forecast, the model was run for 30 years. The wells OB-14, OB-17 and OB-19 drilled in the eastern edge of the reservoir were introduced as injectors. Production was assigned to wells located in the center of the well field (Table 5.3). Although re-injection into the eastern side of the reservoir was able to limit the reservoir pressure decline rate after the first several years, the OB-10 well witnessed a dramatic drop in pressure (91 bars) at the onset of production. However, the other producing wells show a more moderate pressure drop ranging between 24 to 32 bars at the end of the 30 year period, while the pressure drop in well OB-10 reached 108 bars. Due to the limited data currently available, it is not possible to speculate on the different behavior observed in well OB-10. A steady decline in enthalpy was observed, especially in well OB-3 where an enthalpy drop of 64 kJ/kg was observed at the end of the performance prediction run.

The recently drilled wells in the Alangulu area were added to the model to be introduced as injectors in the last three scenarios. In scenario 3, production was assigned to the wells OB-5, OB-6, OB-10, OB-11, OB-14 and OB-17. The injection wells included the AG wells (AG 22-26) and well OB-9. The total production is 2520 tph while injection is 2015 tph. The pressure in the reservoir as monitored through well OB-7 drops 20 bars at the end of the 30 year scenario run, whereas the pressure drop in wells OB-10 and OB-17 is more pronounced as compared to the other production wells reaching 104 bars and 92 bars respectively. A slow and gradual decline in the enthalpy of the producing wells is observed, with the exception of well OB-6, which suffers thermal breakthrough with enthalpy dropping 87 kJ/kg at the end of the forecasting period.

In scenario 4, the producing wells are the same as in scenario 3; injection is continued into the AG wells and OB-9 with the addition of OB-8 as an injector. The mass ratio of injection to production is kept at 0.8. In terms of pressure performance, a gradual decline in the bottom-hole pressure of the producing wells is observed, ranging between 21 bars and 33 bars. However, the pressure drop in OB-10 is again dramatic as observed in previous forecasts, ultimately reaching 103 bars at the end of the forecast run. The enthalpy decline with the exception of OB-6 is more gradual over the 30 year forecast period. A high degree of cooling is observed in well OB-6, where the total decline in enthalpy is 84 kJ/kg.

For the last forecast, production is maintained from the same wells; however injection is limited to the AG wells with no injection into OB-8 and OB-9. The reservoir pressure as represented by well OB-7 drops 22 bars after 30 years. Of the producing wells, the largest pressure drops are observed in wells OB-10 and OB-17, reaching 102 bars and 88 bars respectively. The simulated enthalpy of the producing wells shows a gradual decline, with a maximum enthalpy drop of 37 kJ/kg being observed in well OB-5.

## **CHAPTER 6**

### **CONCLUSIONS**

A numerical simulation model of the Germencik Omerbeyli geothermal field was developed with TOUGH2. To simulate the naturally fractured reservoir, an equivalent model with equivalent fracture relative permeability was used.

A two step calibration process was implemented, first with the static temperature and pressure profiles of the wells and later with the 2006 LTFT data. The permeability distribution structure and mass and heat source were varied iteratively to reach a match between measured and calculated data, the results show that a good match has been obtained. The next step in the simulation study was to carry out several production/injection scenarios to determine the best development strategy for the field.

The simulated data show that the reservoir pressure decline rate decreases after the rapid drop in the first few years. Although the reservoir permeability is high and injection will be important for maintaining production at the present levels, the reservoir appears to have complex flow paths and careful management of injection will be required to prevent thermal breakthrough.

Although injection into the eastern side of the reservoir was able to provide good support to the reservoir pressure, it had an adverse effect on the enthalpy of the producing wells as shown in scenario 2. The reservoir pressure dropped 14 bars at the end of 30 years.

Injection into OB-8 was observed to have minimal effect on the overall reservoir pressure drop. In scenario 3 with no injection into OB-8, the reservoir pressure dropped 20 bars at the end of 30 years, while in scenario 4 with injection into OB-8, the reservoir pressure drops 19 bars for the same time period.

The enthalpy decline in scenario 3 and scenario 4 is more gradual over the 30 year forecast time period, with the exception of OB-6 well which is observed to suffer from thermal breakthrough with the enthalpy dropping 87 kJ/kg and 84 kJ/kg respectively at the end of the forecasts run. Review of overall performance shows that injection into OB-9 has a more adverse effect on enthalpy decline when compared with injection into OB-8.

The simulated response of the reservoir in scenario 5 shows the best results with regards to the enthalpy of the producing wells, where a maximum enthalpy drop of 37 kJ/kg is observed in well OB-5. The performance of the reservoir as simulated by scenario 5 shows that the reservoir has the potential to sustain production at current levels for at least the next 30 years.

## **CHAPTER 7**

### **RECOMMENDATIONS**

The modeling design process selected for the numerical simulation study will allow improvements to be made to various aspects of the model as further data becomes available.

Although the simulation model has provided satisfactory results with regards to matching of the available data. Several recommendations can be made to obtain more optimized match results and more realistic modeling of performance prediction runs.

At the moment, little or no data is available regarding the geology of the area outside the well field. It is recommended to add further details regarding the geology of the field, especially outside the well field area, to the model. This will achieve more realistic modeling results.

As a second step, it is recommended that the characteristics of the geothermal fluid geochemistry, such as dissolved solids as well as CO<sub>2</sub> gas content, be added to the model. The model could then be run with the EWASG executable (Batistelli et al, 1997) or any other simulation program capable of handling water, dissolved solids and non condensable gasses.

## REFERENCES

- Akin, S., Yeltekin K., Parlaktuna, M., 2003, “Numerical modeling of Kizildere geothermal field, Turkey”.
- Babadagli, T., Ershagi, I., 1993, “Improved modeling of oil/water flow in naturally fractured reservoirs using effective fracture relative permeability”, SPE 26076.
- Battistelli, A., Calore, C., Pruess, K., 1997, “The simulator TOUGH2/EWASG for modeling geothermal reservoirs with brines and non-condensable gas”, *Geothermics* 26 (4), 437–464.
- Bodvarsson, G.S., Pruess, K., Lippman, M.J., 1986, “Modeling of Geothermal Systems”, *Journal of Petroleum Technology*, September 1986.
- Dagan, G., Neuman, S.P. (Eds.), 1997, “Subsurface Flow and Transport: A Stochastic Approach”, Cambridge University Press, New York.
- Doe, T.W., Uchida, M., Kindred, J.S., Dershowitz, W.S., 1990, “Simulation of dual porosity flow in discrete fracture networks”, Annual Technical Meeting, Calgary.
- Doughty, C., Bodvarsson, S., 1988, “Some Design Considerations for the Proposed Dixie Valley Tracer Test”, Lawrence Berkeley Laboratory, Berkeley, California, Report: LBL-25971.
- Ercan, A., Sahin, Hudevendigar, 1999, “Hot parts of Germencik geothermal field”, *JEOFIZIK* 13, 51-70.

Filiz, S., Tarcan, G., Gemici, U., 2000, “Geochemistry of the Germencik geothermal fields, Turkey”, Proceedings World Geothermal Congress, Japan.

Finsterle, S., Pruess, K., 1995, “Solving the estimation-identification problem in two-phase flow modeling”, Water Resources Research 31(4), 913–924.

Gelhar, L.W., 1993, “Stochastic Subsurface Hydrology”, Prentice-Hall, Englewood Cliffs, NJ.

Gok, I.M., Sarak, H., Onur, M., Serpen, U., Satman, A., 2005, “Numerical modeling of the Balcova-Narlidere Geothermal field, Turkey”, Proceedings World Geothermal Congress, Japan.

Grant, M.A., Donaldson, I.G., Bixley, P.F., 1982, “Geothermal Reservoir Engineering”, Academic Press, New York.

Hanano, M., Seth, M.S., 1995, “Numerical modeling of hydrothermal convection systems including super-critical fluid”, Proceedings World Geothermal Congress, Florence, 1995, pp. 1681–1686.

Hu, B., 1995, “Reservoir simulation of the Yangbajian geothermal field in Tibet, China.”, Proceedings World Geothermal Congress, Florence, 1995, pp. 1691–1695.

Ingebritsen, S., Sorey, M., 1985, “Quantitative analysis of the Lassen hydrothermal system, northcentral California”, Water Resources Research 21(6), 853–868.

Lippmann, M.J., Bodvarsson, G.S., 1983, “Numerical studies of the heat and mass transport in the Cerro Prieto geothermal field, Mexico”, Water Resources Research 19 (3), 753–767.

Lippmann, M.J., Bodvarsson, G.S., 1985, "The Heber geothermal field, California: natural state and exploitation modeling studies", *Journal of Geophysical Research* 90 (B1), 745–758.

McGuinness, M.J., White, S.P., Young, R.M., Ishizaki, H., Ikeuchi, K., Yoshida, Y., 1995, "A model of the Kakkonda geothermal reservoir", *Geothermics* 24, 1–48.

Nakanishi, S., Iwai, N., 2000, "Reservoir simulation study of the Onikobe geothermal field, Japan", *Proceedings World Geothermal Congress, Kyushu-Tohoku, Japan, May 28–June 10, 2000*, pp. 2159–2164.

Nakanishi, S., Kawano, Y., Todaka, N., Akasaka, C., Yoshida, M., Iwai, N., 1995b, "A reservoir simulation of the Oguni geothermal field, Japan, using MINC type fracture model", *Proceedings World Geothermal Congress, Florence, 18–31 May 1995*, pp. 1721–1726.

Narasimhan, T.N., Witherspoon, P.A., 1976, "An Integral Finite Difference method for analyzing fluid flow in porous media", *Water Resources Research*, 12, 57-64.

O'Sullivan, M.J., 1985, "Geothermal reservoir simulation", *Energy Research* 9, 313–332.

O'Sullivan, M.J., 1987, "Modeling of enthalpy transients for geothermal well", *Proceedings of the 9th New Zealand Geothermal Workshop, University of Auckland, New Zealand, November 1987*, pp. 121–125.

O'Sullivan, M.J., Barnett, B.G., Razali, M.Y., 1990, "Numerical simulation of the Kamojang geothermal field, Indonesia", *Transactions Geothermal Resources Council* 14, 1317–1324.

O'Sullivan, M.J., Bodvarsson, G.S., Pruess, K., Blakeley, M.R., 1985, "Fluid and heat flow in gas-rich geothermal reservoirs", *Society of Petroleum Engineers Journal* 25 (2), 215–226.

O'Sullivan, M.J., Bullivant, D.P., Follows, S.E., Mannington, W.I., 1998, "Modeling of the Wairakei - Tauhara geothermal system", *Proceedings of the TOUGH Workshop '98, Berkeley, California, 4–6 May 1998*, pp. 1–6.

O'Sullivan, M. J., Pruess, K., Marcelo, J. L., 2001, "State of the art of geothermal reservoir simulation", *Geothermics* 30 (2001) 395–429.

Ozgun, N., Pekdeger, A., Wolf, M., Stichler, W., Seiler, K.P., Satir, M., 1998, "Hydrogeochemical and isotope geochemical features of the thermal waters of Kizildere, Salavatli, and Germencik in the rift zone of the Büyük Menderes, western Anatolia, Turkey: Preliminary studies", *Water-Rock Interaction, Arehart & Hutston (eds), Balkema, Rotterdam*.

Parini, M., Cappetti, G., Laudiano, M., Bertani, R., Monterrosa, M., 1995, "Reservoir modeling study of the Ahuachapan geothermal field (El Salvador) in the frame of a generation stabilization project", *Proceedings World Geothermal Congress '95, Florence, 18–31 May 1995*, pp. 1543–1548.

Parini, M., Acuna, J.A., Laudiano, M., 1996, "Reinjected water return at Miravalles geothermal reservoir, Costa Rica: numerical modeling and observations", *Proceedings of the 21st Workshop on Geothermal Reservoir Engineering, Stanford University, Stanford, California, 22–24 January 1996*, pp. 127–134.

Pritchett, J.W., 1995, "STAR: A geothermal reservoir simulation system", *Proceedings World Geothermal Congress '95, Florence*, pp. 2959–2963.

Pruess, K., 1990b, "TOUGH2– A General Purpose Numerical Simulator for Multiphase Fluid and Heat flow", Report: LBL-29400, Lawrence Berkeley Laboratory, Berkeley, California.

Pruess, K., Finsterle, S., Moridis, G., Oldenburg, C., Wu, Y., 1997, "General Purpose Reservoir Simulators: the TOUGH2 Family", Geothermal Resources Council, 26:2, pp. 53-57

Pruess, K., Oldenburg, C., Moridis, G., 1999, "TOUGH2 User's Guide, Version 2.0", Lawrence Berkeley National Laboratory, Berkeley, California, LBNL-43134.

Pruess, K., Weres, O., Schroeder, R., 1983, "Distributed parameter modeling of a producing vapor-dominated geothermal reservoir", Water Resources Research 19 (5), 1219–1230.

Pruess, K., Oldenburg, C., Moridis, G., 1998, "An overview of TOUGH2, Version 2.0", Proceedings of the TOUGH Workshop '98, Berkeley, California, pp. 307–314.

Pruess, K., Narasimhan, T.N., 1985, "A practical method for modeling fluid and heat flow in fractured porous media", SPE Journal 25 (1), 14–26.

Simsek, S., 2003, "Hydrogeological and isotopic survey of geothermal fields in the Buyuk Menderes graben, Turkey", Geothermics 32, 669-678.

Simsek, S., 2006, "Aydin–Germencik geothermal field geology and hydrogeological potential evaluation report".

Sarkar, S., Toksoz, N., Burns, D.P., "Fluid flow simulation in fractured reservoirs".

Serpen, U., Yamanlar, S., Karamandersi, I.H., 2000, "Estimation of geothermal potential of Buyuk Menders region in Turkey", Proceedings World Geothermal Congress, Japan.

Swenson, D., hardeman, B., Butler, S., Persson, C., Thornton, C., “Using the Petrasim pre- and post-processor for TOUGH2, TETRAD and STAR”.

Uraz, I., Akin, S., 2003, “Optimization of reinjection in geothermal reservoirs”, Proceedings, Twenty Eighth Workshop on Geothermal Reservoir Engineering, Stanford University, California, January 27-29, 2003.

Vengosh, A., Helvaci, C., Karamanderesi, I.H., 2002, “Geochemical constraints for the origin of thermal waters from western Turkey”, Applied Geochemistry 17 (2002), pp.163-183.

Vinsome, P.K.W., Shook, G.M., 1993, “Multi-purpose simulation”, Journal of Petroleum Science and Engineering 9 (1), pp. 29–38.

Voss, C. I., 1984, “SUTRA: A Finite-Element Simulation Model for Saturated-Unsaturated Fluid-Density-Dependent Ground-Water Flow with Energy Transport or Chemically-Reactive Single-Species Solute Transport”, U.S. Geological Survey Water-Resources Investigations, Report 84-4369.

Warren, J.E., and Root, P., 1963, “The Behavior of Naturally Fractured Reservoirs”, Society of Petroleum Engineers Journal, pp. 245-255.

White, S.P., Young, R.M., Kissling, W.M., 1998, “Using ITOUGH2 to improve geothermal reservoir models”, Proceedings of the TOUGH Workshop ‘98, Berkeley, California, 1998, pp. 25–29.

Yamaguchi, S., Akibayashi, S., Rokugawa, S., Fujinaga, Y., Tenma, N., Sato, Y., 2000, “The numerical modeling study of the Hijiori HDR test site”, Proceedings World Geothermal Congress, Japan, 2000, pp. 3975–3980.